



# Competition between Persistent Na<sup>+</sup> and Muscarine-Sensitive K<sup>+</sup> Currents Shapes Perithreshold Resonance and Spike Tuning in CA1 Pyramidal Neurons

Jorge Vera, Julio Alcayaga\* and Magdalena Sanhueza\*

Department of Biology, Cell Physiology Center, University of Chile, Santiago, Chile

## OPEN ACCESS

### Edited by:

Arianna Maffei,  
Stony Brook University, USA

### Reviewed by:

Thierry Ralph Nieus,  
Luigi Sacco Hospital, Italy  
Rory McQuiston,  
Virginia Commonwealth University,  
USA  
Dominique Debanne,  
University of the Mediterranean,  
France

### \*Correspondence:

Julio Alcayaga  
jalcayag@uchile.cl  
Magdalena Sanhueza  
masanhue@uchile.cl

Received: 09 December 2016

Accepted: 22 February 2017

Published: 08 March 2017

### Citation:

Vera J, Alcayaga J and Sanhueza M  
(2017) Competition between  
Persistent Na<sup>+</sup> and  
Muscarine-Sensitive K<sup>+</sup> Currents  
Shapes Perithreshold Resonance and  
Spike Tuning in CA1 Pyramidal  
Neurons. *Front. Cell. Neurosci.* 11:61.  
doi: 10.3389/fncel.2017.00061

Neurons from many brain regions display intrinsic subthreshold theta-resonance, responding preferentially to theta-frequency oscillatory stimuli. Resonance may contribute to selective communication among neurons and to orchestrate brain rhythms. CA1 pyramidal neurons receive theta activity, generating place fields. In these neurons the expression of perithreshold frequency preference is controversial, particularly in the spiking regime, with evidence favoring either non-resonant (integrator-like) or resonant behavior. Perithreshold dynamics depends on the persistent Na<sup>+</sup> current  $I_{NaP}$  developing above  $-70$  mV and the muscarine-sensitive K<sup>+</sup> current  $I_M$  activating above  $-60$  mV. We conducted current and voltage clamp experiments in slices to investigate perithreshold excitability of CA1 neurons under oscillatory stimulation. Around 20% of neurons displayed perithreshold resonance that is expressed in spiking. The remaining neurons ( $\sim 80\%$ ) acted as low-pass filters lacking frequency preference. Paired voltage clamp measurement of  $I_{NaP}$  and  $I_M$  showed that perithreshold activation of  $I_M$  is in general low while  $I_{NaP}$  is high enough to depolarize neurons toward threshold before resonance expression, explaining the most abundant non-resonant perithreshold behavior. Partial blockade of  $I_{NaP}$  by pharmacological tools or dynamic clamp changed non-resonant to resonant behavior. Furthermore, shifting  $I_M$  activation toward hyperpolarized potentials by dynamic clamp also transformed non-resonant neurons into resonant ones. We propose that the relative levels of  $I_{NaP}$  and  $I_M$  control perithreshold behavior of CA1 neurons constituting a gating mechanism for theta resonance in the spiking regime. Both currents are regulated by intracellular signaling and neuromodulators which may allow dynamic switching of perithreshold behavior between resonant and non-resonant.

**Keywords:** resonance, oscillations, intrinsic excitability, persistent sodium current, muscarine-sensitive potassium current, hippocampal neurons

## INTRODUCTION

Many cognitive and behavioral processes like memory and navigation depend on hippocampal function and rely on network oscillatory activity at frequencies around 4–10 Hz, also known as the theta range (O'Keefe and Recce, 1993; Buzsáki, 2002, 2005; Lisman, 2005). Principal neurons from hippocampal CA1 region are endowed with intrinsic properties that favor activity

at theta frequency, displaying an increased subthreshold voltage response for rhythmic stimulation in the theta range, thus acting as resonators (Hu et al., 2002). This selective voltage response or frequency preference is the result of active and passive mechanisms. Specific slowly-activating membrane currents produce an active attenuation of low-frequency voltage responses, while the passive properties of the cellular membrane filter out high-frequency oscillations (Hutcheon and Yarom, 2000). This generates a band-pass filtering effect that tunes the voltage response of resonant neurons around a specific frequency of inputs (Izhikevich, 2002). This frequency selectivity is revealed by a bell-shaped impedance profile that reaches a peak ( $Z_{\text{Max}}$ ) at the resonant frequency,  $f_R$ . Resonance strength is quantified by the Q-value corresponding to the ratio between  $Z_{\text{Max}}$  and the impedance at 0.5 Hz (Hutcheon et al., 1996).

CA1 pyramidal neurons possess two complementary mechanisms to produce subthreshold theta resonance at hyperpolarized or depolarized potentials (Hu et al., 2002, 2009). Below  $-70$  mV, frequency preference is generated by the hyperpolarization-activated cationic current,  $I_h$ , a mixed  $\text{Na}^+$  and  $\text{K}^+$  current that activates at membrane potentials below  $-70$  mV (Biel et al., 2009). This current is expressed in an increasing gradient distal from the soma, providing a strong low-frequency filter at dendrites (Magee, 1998).

The mechanism described for subthreshold theta-resonance above  $-70$  mV relay on two voltage-dependent currents widely present in the mammalian brain: the muscarine-sensitive  $\text{K}^+$  current,  $I_M$  (Shah et al., 2002) that produces the actual filter of low frequency oscillations and therefore is called a resonant current (Izhikevich, 2002), and the persistent  $\text{Na}^+$  current,  $I_{\text{NaP}}$ , (Crill, 1996) that increases the amplitude of voltage fluctuations acting as an amplifying current (Gutfreund et al., 1995; D'Angelo et al., 1998, 2001).

$I_M$  is a slow activating/non inactivating voltage-sensitive  $\text{K}^+$  outward current that activates at membrane potentials above  $\sim -70$  mV (Halliwell and Adams, 1982). It depends on the KCNQ2/3 channel, mostly restricted to the somatic region (Wang et al., 1998; Hu et al., 2007).

In turn,  $I_{\text{NaP}}$  is a relatively fast-activating ( $\sim 1$  ms) voltage-sensitive current that activates at potentials above  $-70$  mV, presents a very slow inactivation and is also located in the soma of pyramidal neurons (French et al., 1990; Colombo et al., 2013). This current amplifies subthreshold voltage oscillations in resonant and non-resonant neurons (Hutcheon and Yarom, 2000; Vera et al., 2014). Importantly, elevated  $I_{\text{NaP}}$  levels due to mutations can trigger epileptogenic activity (Kearney et al., 2001), indicating the relevance of  $I_{\text{NaP}}$  in physiological and pathological conditions (Stafstrom, 2007).

Aside the well-documented individual contribution of  $I_M$  and  $I_{\text{NaP}}$  to neuron excitability at subthreshold voltages, the joint contribution of these currents to shape perithreshold dynamics remains poorly understood. The similar voltage range of activation and the opposed effects on membrane potential of these currents, together with a high degree of modulation by second messengers and neuromodulators (Crill, 1996; Marrion, 1997), place the combination of the two currents as a feasible and sophisticated mechanism to control perithreshold dynamics.

Perithreshold resonance is not always observed (discussed in Hu et al., 2002) and the general use of tetrodotoxin (TTX) to avoid contamination of recordings with spikes (and also eliminating  $I_{\text{NaP}}$ ) occludes the possibility to evaluate if frequency preference is translated to the firing regime (Hu et al., 2002). In addition, it is often considered that hippocampal pyramidal neurons behave only as integrators under *in vitro* conditions (Prescott et al., 2008). Therefore, it is still unclear whether CA1 neurons can express perithreshold resonance and impact firing.

To understand the mechanism that controls perithreshold excitability, we conducted a comprehensive study of the contribution of  $I_M$  and  $I_{\text{NaP}}$  to oscillatory processing using whole-cell recordings in current clamp, voltage clamp, and dynamic clamp, and computational modeling.

We found that CA1 pyramidal neurons display a differential behavior at perithreshold voltage range due to a heterogeneous contribution of  $I_{\text{NaP}}$  and  $I_M$ . Reducing  $I_{\text{NaP}}$  or increasing  $I_M$  switches non-resonant neurons to resonant, which suggest that perithreshold frequency preference depends on the dynamic interaction between  $I_{\text{NaP}}$  and  $I_M$ .

## METHODS

Animal care and experimental procedures were approved by the Bio-Ethical Committee of the Facultad de Ciencias, Universidad de Chile, according to the ethical rules of the Biosafety Policy Manual of the Fondo Nacional de Desarrollo Científico y Tecnológico (FONDECYT), Chile.

### Slice Preparation

Male Sprague Dawley rats, from 18 to 30 days-old, were anesthetized and decapitated. The brain was rapidly removed and transferred to an ice-cold dissection solution containing (in mM): 206 sucrose, 2.8 KCl, 1  $\text{MgCl}_2$ , 2  $\text{MgSO}_4$ , 1  $\text{CaCl}_2$ , 26  $\text{NaHCO}_3$ , 1.125  $\text{NaH}_2\text{PO}_4$ , 10 glucose, and 0.4 ascorbic acid (equilibrated with 95%  $\text{O}_2$  and 5%  $\text{CO}_2$ ), pH 7.3. Septotemporal slices (400  $\mu\text{m}$ ) containing dorsal hippocampus, were obtained with a vibratome (Vibratome Sectioning System 102, Pelco, USA). Slices were placed in a holding chamber with standard artificial cerebro-spinal fluid (ACSF) and were left to recover during at least 1 h at  $30^\circ\text{C}$  before using them for recordings.

### Electrophysiological Recordings

Whole cell patch-clamp recordings were conducted under visual guidance with an upright microscope (Nikon Eclipse E600FN, Nikon Corp. Instruments Co., Japan) equipped with oblique infrared and DIC optics. Electrodes (2.5–3.0 and 3.5–4.0  $\text{M}\Omega$  for voltage and current-clamp experiments, respectively) were fabricated from borosilicate glass capillary tubing ( $0.8\text{--}1.10 \times 100$  mm; Kimble Glass Inc., USA) using a horizontal puller (Flaming/Brown P-97, Sutter Instrument Co., USA). Current-clamp and voltage-clamp recordings were made with an EPC-10 patch-clamp amplifier (Heka, Heidelberg, Germany); signals were filtered at 10 kHz and acquired 25 kHz using the Heka Patchmaster software. In voltage-clamp experiments series resistance was compensated by 60–70%. Only cells with a stable resting membrane potential negative to  $-60$  mV were used

for recordings. Spike threshold was measured either during stimulation with a current ramp (8 pA/ms; from  $-80$  mV until firing) or during the application of a pseudo-sinusoidal current of linearly increasing frequency and constant amplitude (ZAP stimulus). Threshold was defined as the membrane potential for which the time derivative exceeded 5 mV/ms.

All experiments were performed in presence of 10  $\mu$ M CNQX and 100  $\mu$ M PTX to block AMPA-R and GABA<sub>A</sub>-R mediated currents. In some experiments 100  $\mu$ M APV was also added.

CA1 pyramidal neurons were identified morphologically by their soma located in the stratum pyramidale that extend to stratum radiatum with a prominent apical dendrite. Once in whole-cell configuration was confirmed a resting membrane potential below  $-70$  mV ( $-81.5 \pm 0.8$  mV,  $n = 32$ ) and input resistance at  $-80$  mV near 60 M $\Omega$  ( $55.9 \pm 2.3$  M $\Omega$ ,  $n = 32$ ).

### Recording Solutions (in mM):

Artificial cerebro-spinal solution (ACSF) contained (in mM): 124 NaCl, 2.8 KCl, 1.25 NaH<sub>2</sub>PO<sub>4</sub>, 26 NaHCO<sub>3</sub>, 10 Glucose, 2 MgCl<sub>2</sub>, 2 CaCl<sub>2</sub>, and 0.4 ascorbic acid (equilibrated with 95% O<sub>2</sub> and 5% CO<sub>2</sub>), pH 7.3 and 285–295 mOsm.

Low Na<sup>+</sup> ACSF (in mM): 38 NaCl, 80 NMDG, 80 HCl, 2.8 KCl, 1.25 NaH<sub>2</sub>PO<sub>4</sub>, 26 NaHCO<sub>3</sub>, 10 Glucose, 2 MgCl<sub>2</sub>, 2 CaCl<sub>2</sub>, and 0.4 ascorbic acid (equilibrated with 95% O<sub>2</sub> and 5% CO<sub>2</sub>), pH 7.3 and 285–295 mOsm.

Internal pipette solution was based in previous works reporting stability of resting membrane potential, action potential threshold, and after-potential depolarization (Xu et al., 2005; Kaczorowski et al., 2011), in mM: 123 K-Gluconate, 10 KCl, 4 Glucose, 1 EGTA, 10 HEPES, 2 Na<sub>2</sub>ATP, 0.2 Na<sub>3</sub>GTP, 10 phosphocreatine, 1 MgCl<sub>2</sub>, 0.1 CaCl<sub>2</sub>, and 0.1% biocytin, pH 7.35, and 285–290 mOsm.

### Liquid Junction Potential (LJP)

We measured the LJP between pipette solution and both ACSF ( $\sim 13$  mV) and low Na<sup>+</sup> ACSF ( $\sim 17.5$  mV), according to the procedure described by Neher (1992), and recorded values were corrected offline during analyses.

### ZAP Stimulation and Analysis

Voltage responses to an intracellularly injected pseudo-sinusoidal current of linearly decreasing or increasing frequency and constant amplitude (10 pA) (ZAP stimulus; frequency interval: 0–15 or 20 Hz, 10 s duration) were recorded in current clamp conditions. In experiments with blockers of voltage-dependent channels the amplitude of ZAP stimuli was adjusted to maintain a peak to peak voltage response comparable to the control condition (5–10 mV) and to favor the evaluation of perithreshold resonance in the absence of spikes. In all experiment the protocol was repeated 8–10 times in every neuron, for each condition. The output equipotential subthreshold waves were averaged to proceed with the impedance analysis.

The impedance frequency profile ( $Z(f)$ ) was obtained from the output (voltage) and input (current) waves Fast Fourier Transforms (FFT) ratio ( $Z(f) = FFT[V(t)]/FFT[I(t)]$ ). The impedance is a complex quantity ( $Z(f) = Z, Real + Z, Imaginary$ ),

where the real part ( $Z, Real$ ) is the resistance and the imaginary part ( $Z, Imaginary$ ), the reactance. For each given frequency, the complex impedance can be plotted as a vector with magnitude ( $|Z(f)|$ ) and phase. We only focused on the effects on impedance magnitude obtained with the following expression.

$$|Z(f)| = \sqrt{(Z, Real)^2 + (Z, Imaginary)^2} \quad (1)$$

Throughout the text the term *impedance* will be used to refer to the magnitude of the impedance vector, unless otherwise stated. Frequencies below 0.5 Hz were not plotted in the impedance profiles graphs, to avoid low frequency distortions. Off-line analyses and graphs were performed with Igor Pro 6.2 software (WaveMetrics Inc., USA).

### Quantification of Resonance

Resonance is defined as the band-pass filter property of the impedance profile (Hutcheon and Yarom, 2000). The Q factor or value is a measure of resonance strength and is quantified as the ratio between the maximal impedance (i.e., the impedance at the resonance frequency,  $|Z(f_{res})|$ ) and the impedance at the lowest frequency ( $|Z(0.5)|$ ) (Hutcheon et al., 1996). Here we used  $Q = 1$  in the subthreshold depolarized voltage response as a criterion to define non-resonant behavior. To quantify resonance from recordings containing action potentials we defined an apparent Q value (Q'-value) using as point of reference the impedance at 1 Hz (Figures 2, 6) and 2 Hz (Figure 7) instead of 0.5 Hz, to discard suprathreshold contribution of spike firing to impedance profile.

### Firing Probability Measurements

Firing probability under ZAP stimulation was computed for each oscillatory period as the number of sweeps in which neurons fired a spike divided by the total number of sweeps (typically 8). The frequency of stimulation associated to each depolarized excursion was the frequency at the peak of each current oscillation (starting near 1.2 up to 20 Hz). For instance, if a neuron fired a spike at a given frequency in 4 out of 8 sweeps, its firing probability at that frequency is 0.5.

### Voltage Clamp Measurement of $I_{NaP}$ and $I_M$

Despite technical limitations of whole-cell voltage clamp technique on neurons with complex morphology, numerous studies have shown that single-electrode voltage-clamp measurement of whole cell currents is suitable for recording in brain slices, including kinetics and voltage sensitivity of  $I_{NaP}$  and  $I_M$  (Halliwell and Adams, 1982; French et al., 1990; Hu et al., 2009). However, it is necessary to be aware of the lack of space-clamp control and its effects on regions distal to the soma. Three reasons support an acceptable quality of our measurements. First, both  $I_{NaP}$  and  $I_M$  are conductances located mainly at the soma where space-clamp control is possible. Second, the current injection needed for depolarizing to perithreshold potential is low (below 800 pA), reducing the error of our measurements. In addition, the reduction of Na<sup>+</sup> driving force together with a slow ramp protocol allows inactivation of  $I_{NaT}$  and a low amplitude and well-clamped  $I_{NaP}$  recording. And third, most of our conclusions are taken from a relative comparison of  $I_{NaP}$  and

$I_M$ , with both currents sequentially recorded in the same cell, with the same pipette under the same conditions, thus decreasing possible bias due to different experimental configurations.

Furthermore, our voltage clamp data agree with values recorded in dissociated neurons (French et al., 1990), with voltage dependent behavior of neurons recorded in current clamp (Figures 2, 3) and also our voltage clamp data is able to reproduce voltage dependent behavior of neurons when are used to feed the computational models (Figure 5).

## Fitting Curves

To characterize voltage dependence of  $G_{NaP}$  and  $G_M$  we fitted the following sigmoid curve:

$$G_i(V) = G_{Max} \frac{1}{1 + e^{-\frac{V-V_{0.5}}{s}}} \quad (2)$$

$G_{Max}$  is the maximal conductance,  $V_{0.5}$  is the voltage for half activation and  $s$  is the slope of voltage sensitivity. Despite experimental curves for  $G_M$  did not reach saturation, fitting values allowed a good mathematical characterization of conductance curve at the voltage range of interest.

## Computer Simulations

To explore perithreshold behavior of neurons recorded under voltage-clamp we developed a point process conductance-based model following the Hodgkin-Huxley equations (Hodgkin and Huxley, 1952). The model included a passive leak current ( $I_{Leak}$ ), a persistent (non-inactivating)  $Na^+$  current ( $I_{NaP}$ ) (French et al., 1990) and the slow muscarine-regulated  $K^+$  current,  $I_M$  (Adams et al., 1982). The model did not include a firing mechanism (fast sodium and potassium conductances).

The equation describing the evolution of membrane voltage (V) in time is

$$C \frac{dV}{dt} = I_{ZAP} - I_{Leak} - I_M - I_{NaP} \quad (3)$$

where  $C$  is the membrane capacitance estimated for each cell from the capacitive current elicited with a  $-5$  mV step at  $-70$  mV holding potential in voltage clamp configuration (Golowasch et al., 2009), and  $I_{ZAP}$  is the applied current. Intrinsic ionic currents in Equation 3 follow the next set of equations

$$I_{Leak} = G_{Leak}(V - E_{Leak}) \quad (4)$$

$$I_{NaP} = G_{NaP}w(V - E_{Na}) \quad (5)$$

$$I_M = G_M r(V - E_K) \quad (6)$$

where  $G_{Leak}$ ,  $G_M$  and  $G_{NaP}$  are the maximal conductances of the corresponding currents and  $E_{Leak}$ ,  $E_K$ , and  $E_{Na}$  the reversal potentials of  $I_{Leak}$ ,  $K^+$ - and  $Na^+$ -mediated currents, respectively, and  $r$ ,  $w$  are the state variables (see below).  $E_{Leak}$  was set to  $-70$  mV,  $E_K$  ( $-99$  mV) and  $E_{Na}$  ( $47.1$  mV) were calculated from the ionic conditions in our current clamp recordings. To simulate each recorded neuron, maximal conductance and steady-state values for  $I_{NaP}$  and  $I_M$  were obtained by fitting a sigmoid curve from experimental data (Figure 4) as explained above. This gave us a specific set of parameters for each neuron from  $-70$  to  $-40$

mV, allowing a precise characterization of voltage dependence at perithreshold region.

The dynamics of the state variables  $x_i = r$  and  $w$  is ruled by the following equation:

$$\frac{dx_i}{dt} = \frac{x_{i\infty}(V) - x_i}{\tau_{x_i}(V)} \quad (7)$$

where  $x_{i\infty}$  are the steady-state values of  $x_i$ , and  $\tau_{x_i}$  are the corresponding time constants.

The time constant for  $I_{NaP}$  ( $\tau_{NaP}$ ) was set at 1 ms according to Vervaeke et al. (2006) and for  $I_M$  was modeled according to the voltage dependent equation (Adams et al., 1982):

$$\tau_M = \frac{1000}{3.3(e^{(V+35)/40} + e^{-(V+35)/20})} \quad (8)$$

and was divided by the temperature-correcting factor  $3^{(T-22)/10}$  (Hodgkin and Huxley, 1952) to set simulations at  $35^\circ\text{C}$ .

Simulations were performed using Igor Pro 6.2 software on a Mac Book Pro (Apple Inc., USA) computer. An integration time step of  $10 \mu\text{s}$  ( $100$  kHz) was used for all simulations. The stimulation protocol used in all the cases comprised sequential ZAP current injections, each of 10 s duration and 5 pA amplitude, and ranging from 0 to 20 Hz. The ZAP injections were superposed to increasing holding current steps that moved the average potential between  $\sim -70$  and  $-35$  mV, as in the electrophysiological current-clamp experiments. The code for reproducing the computer simulations described in this paper is available upon request to authors.

## Dynamic Clamp

For dynamic-clamp experiments, the current-clamp amplifier was driven by an analog signal from a desktop computer running Real-Time Linux Dynamic Clamp (Real-Time Experimental Interface, RTXI Dorval et al., 2001; Bettencourt et al., 2008) using an update frequency of 25 KHz.

Dynamic current used to decrease endogenous  $I_{NaP}$  or increase  $I_M$ , were introduced via dynamic clamp using Equations (5) and (6), where  $V$  is the online measured membrane potential. The dynamics of the state variables  $w$  and  $r$  were modeled according to Equation (7). The voltage dependence of the state variables at equilibrium was given by the equations:

$$w_\infty = \frac{1}{1 + e^{-(V+V_{0.5})/5}} \quad (9)$$

$$r_\infty = \frac{1}{1 + e^{(V+35)/10}} \quad (10)$$

where  $V$  is the online recorded membrane potential and  $V_{0.5}$  is the potential for half activation of  $I_{NaP}$ . Here we set  $V_{0.5}$  as  $-52$  mV according to our average voltage-clamp measurement (Figure 4).

The time constant for  $I_{NaP}$ ,  $\tau_{NaP}$ , was set at 1 ms according to Vervaeke et al. (2006) and for  $I_M$  was modeled according to Equation (8).

Here we show dynamic currents as the external current that was injected to neurons, following the standard convention were positive currents are depolarizing and negative currents are hyperpolarizing.



## Statistical Analysis

Statistical analysis was performed in GraphPad Prism 6.07 (GraphPad Software, Inc, USA). Group data is presented as the mean  $\pm$  standard error together with the sample size of cells ( $n$ ). For data with normal distribution (as  $Z_{\max}$ , resting potential,  $R_{\text{in}}$ ,  $G_{\max}$ ,  $G_{(V)}$ , or  $I_{(V)}$ ) we used different parametric tests. When data structure was a single variable measured at different membrane potentials and we needed to compare non-resonant vs. resonant cells (Figure 1) or non-resonant cells in control conditions vs. drug (Figures 3, 4), or the firing probability as function of stimulation frequency in the different experimental conditions (Figures 6, 7), we used two-way repeated measures ANOVA with Holm-Šidák's multiple comparison test. When comparing data at a single membrane potential between non-resonant and resonant cells we used Student's  $t$ -test (Figure 2). When comparing data at different conditions and a single membrane potential (Figures 6, 7) we used one-way ANOVA with matched samples and Tukey's multiple comparison tests.

When comparing  $Q$  or  $Q'$  values we used a non-parametric Mann-Whitney rank test for unpaired data (Figures 1, 2), Wilcoxon rank test for paired data (Figure 3) and Friedman test with Dunn's multiple comparison test to evaluate the effect of PHT and dynamic clamp manipulations (Figures 6, 7). Most statistical tests were two-tailed with exception of those comparing non-resonant vs. resonant data in Figure 2. We used  $\alpha = 0.05$  as critic value.

## Drugs

Drugs were bath-applied at the following final concentrations: 10  $\mu\text{M}$  6-cyano-7-nitroquinoxaline-2,3-dione (CNQX; AMPA-type glutamate receptor antagonist), 100  $\mu\text{M}$  d-2-amino-5-phosphonovaleric acid (APV; NMDA-type glutamate receptor antagonist), 100  $\mu\text{M}$  picrotoxin (PTX; GABA<sub>A</sub> receptor blocker), 1  $\mu\text{M}$  tetrodotoxin (TTX; voltage-dependent Na<sup>+</sup> channel blocker), 10  $\mu\text{M}$  XE991 (KCNQ channel blocker), 60  $\mu\text{M}$  phenytoin (PHT,  $I_{\text{NaP}}$  blocker). Drugs were obtained from Sigma, except for XE991 purchased from Tocris, and TTX that was obtained from Alomone Labs.

## RESULTS

### A Small Fraction of CA1 Pyramidal Neurons Display Perithreshold Resonance in Slices

Our first approach for investigating the perithreshold behavior of pyramidal neurons was to measure their voltage response to ZAP stimulation under whole cell current clamp. We set the ZAP amplitude to produce a peak-to-peak voltage oscillation of  $\sim 5$ – $8$  mV, while neurons were maintained at different subthreshold potentials by the injection of a stable holding current; for simplicity, we will refer to this potential as “holding potential.” As expected, all CA1 pyramidal neurons displayed resonance at hyperpolarized potentials due to the presence of  $I_h$  (Hu et al., 2002; see below). However, these same neurons presented different behaviors at the perithreshold region, just below the spike threshold. We found that 21 out of 26 of recorded neurons ( $\sim 80\%$ ) behaved as a pure low-pass filters, reaching an average perithreshold holding potential of  $-63.6 \pm 2.8$  mV. In contrast, the remaining  $\sim 20\%$  of them showed

a more depolarized perithreshold potential of  $-62.3 \pm 0.6$  mV ( $P = 0.014$ ) and expressed a strong frequency preference at theta range (Figure 1A). After impedance analysis, we found that the larger group of neurons presented a  $Q = 1$  and  $f_R$  of 0.5 Hz, characteristic of non-resonant neurons (Koch, 1984; Hutcheon et al., 1996). The other group displayed a strong resonant profile, with a  $Q$  of  $1.24 \pm 0.09$  and a  $f_R$  at  $3.5 \pm 1.6$  Hz (Figures 1A–C and raw data in Figure S1), proper of a  $I_M$ -dependent resonance (Hu et al., 2002). Those neurons presenting non-resonant behavior also displayed a higher  $Z_{\max}$ , in agreement with a lack of activated  $I_M$  (Figures 1A–C, raw data in Figure S1). Thus, here we will refer to CA1 neurons as resonant or non-resonant according to their perithreshold behavior.

As mentioned, voltage responses at  $-85$  mV after ZAP stimulus were similar in the two groups of cells, displaying strong  $I_h$ -dependent resonance without differences in  $Q$  value,  $f_R$ , or  $Z_{\max}$  (Figures 1A–C, raw data in Figure S1). When stimulus was applied at  $-70$  mV both groups of neurons showed reduced resonant behavior, together with similar resonant parameters ( $Q$ ,  $f_R$ , and  $Z_{\max}$ , Figures 1A–C, raw data in Figure S1).

To further study the transition from subthreshold to suprathreshold potential, we applied ZAP stimuli just overcoming action potential threshold and quantified the firing probability as a function of frequency (see Section Methods). We found that non-resonant neurons regularly started to fire during the first depolarizing incursion, occurring at 1.2 Hz (Figure 2A upper panel). Resonant neurons displayed higher firing probability at theta range (4–6 Hz), accompanied by a clear attenuation of firing at lower frequencies (Figure 2B). To compare impedance profiles at this suprathreshold region we calculated the  $Q'$  value, using as a reference the impedance at 1 Hz (see Section Methods). While non-resonant neurons maintained a  $Q'$  value near 1 ( $1.06 \pm 0.02$ ) with an average  $f_R$  at  $1.7 \pm 0.2$  Hz, resonant neurons displayed a stronger  $Q'$  value ( $1.35 \pm 0.06$ ) with an average  $f_R$  at  $4.5 \pm 0.2$  Hz (Figures 2C,D). The peak impedance was higher for non-resonant ( $231.3 \pm 22.4$  M $\Omega$ ) than in resonant ( $144 \pm 22.4$  M $\Omega$ ) neurons, while the holding potential necessary to reach spike threshold with ZAP protocol was more hyperpolarized in non-resonant ( $-62.48 \pm 0.7$  mV) than in resonant ( $-60.0 \pm 0.8$  mV) neurons (Figures 2E,F).

Since a more depolarized action potential threshold would depolarize the perithreshold region, we measured the spike threshold using a depolarizing current ramp (see Section Methods). We obtained a slightly more depolarized value for resonant neurons, but without reaching statistical significance ( $-53.6 \pm 0.7$  mV vs.  $-52.2 \pm 1.1$  mV,  $P = 0.19$ ).

### The Expression of Perithreshold M-Resonance Is Occluded in Most Neurons by $I_{\text{NaP}}$ -Driven Low Frequency Firing

The described difference in perithreshold behavior of pyramidal neurons suggests that the conductances involved in resonance in this voltage range,  $I_{\text{NaP}}$  and  $I_M$ , may have different levels of activation in the two populations.

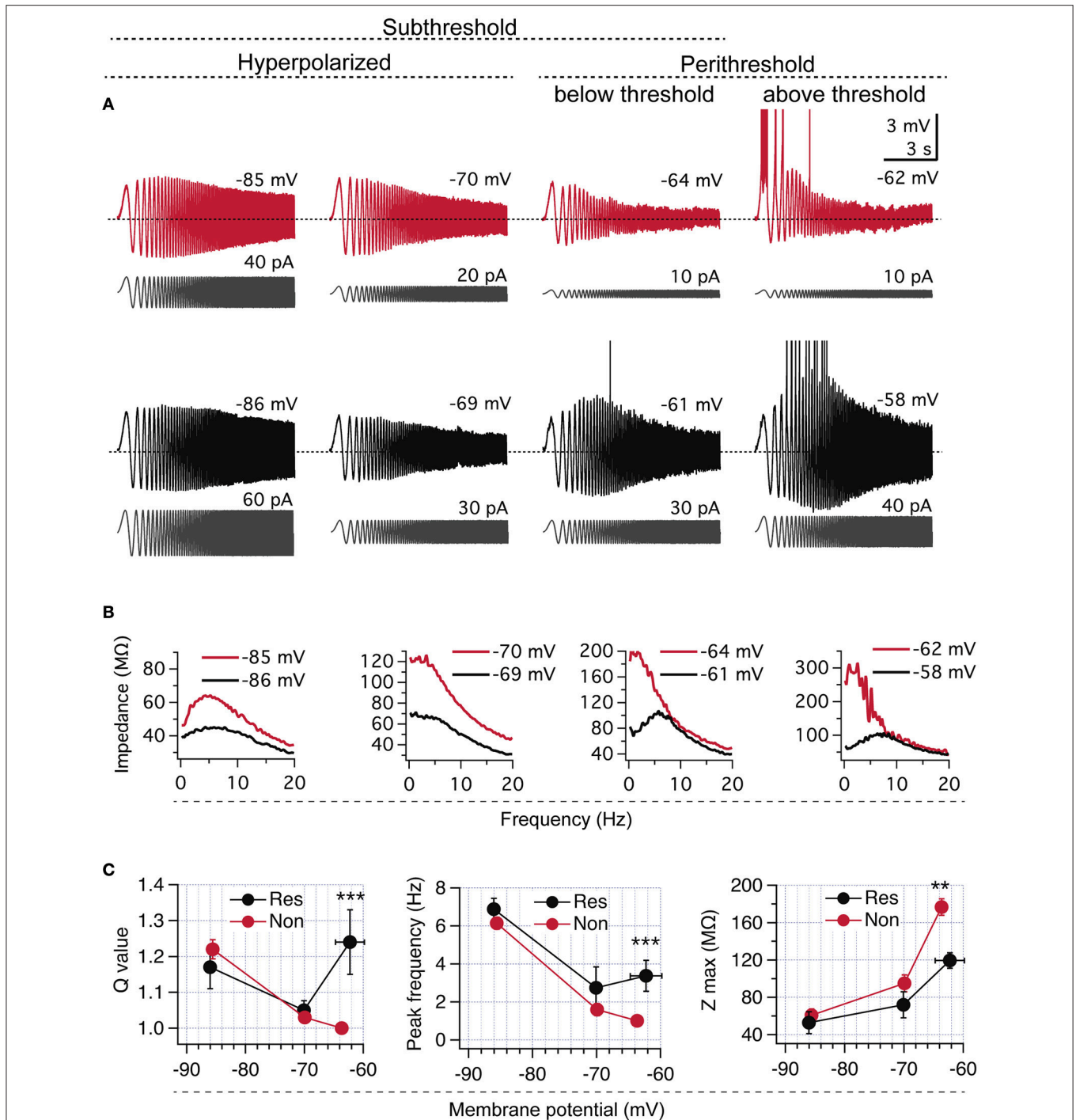
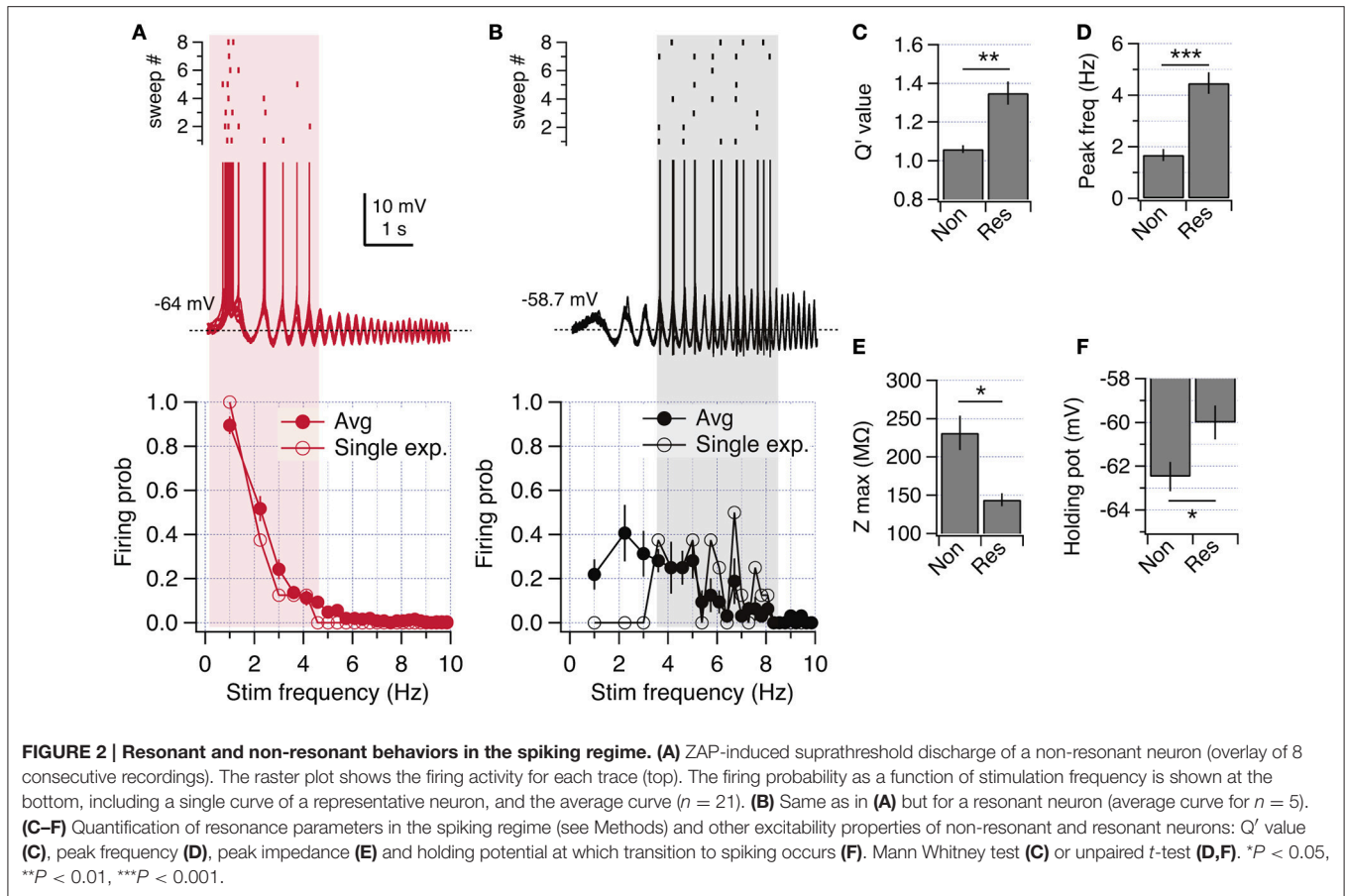


**FIGURE 1 | CA1 pyramidal neurons display two different perithreshold behaviors under oscillatory stimulation. (A)** Voltage responses of two CA1 pyramidal neurons (red and black) stimulated with ZAP protocols (gray) from hyperpolarized (left) to depolarized perithreshold potentials (right; below and above spike threshold). While hyperpolarized responses were similar, cells presented different perithreshold behaviors, non-resonant (red), and resonant (black). **(B)** Impedance profile obtained from recordings in **(A)**. **(C)** Quantification of resonance parameters in the whole subthreshold range for neurons displaying non-resonant (Non,  $n = 21$ ) and resonant (Res,  $n = 5$ ) perithreshold behavior. Mann Whitney test (Q value) and Two-way ANOVA (peak frequency and  $Z_{max}$ ). \*\* $P < 0.01$ , \*\*\* $P < 0.001$ .

To evaluate this possibility, we explored the ZAP-induced voltage response at depolarized potentials (up to  $-45$  mV with 5 mV steps) in non-resonant neurons in presence of the

selective  $\text{Na}^+$  channel blocker tetrodotoxin (TTX) to avoid spike generation. Interestingly, at voltages above  $-55$  mV all studied neurons displayed strong resonant behavior, with Q



values higher than 1.4 and  $f_R$  above 4 Hz (**Figure 3**), even though they were non-resonant near  $-60$  mV. To corroborate that the observed resonant behavior was consequence of  $I_M$  activation we bath-applied the selective M-channel blocker XE991, which consistently eliminated resonance at depolarized potentials, but not at hyperpolarized potentials (**Figure 3**).

These experiments show that M-resonance consistently appears in all neurons at voltages more depolarized than  $-55$  mV (see also Hu et al., 2002), which in most cases is above the spike threshold.

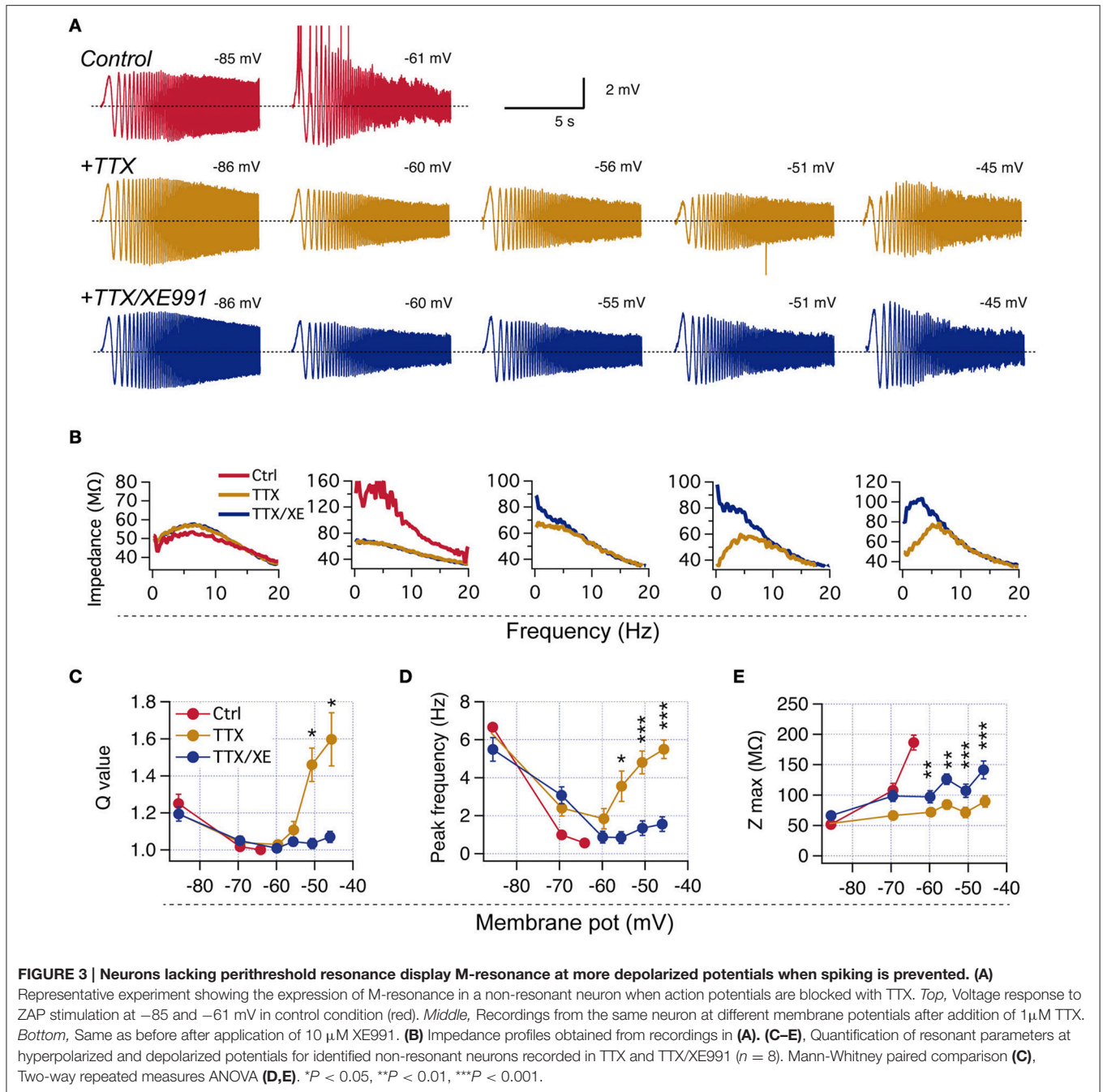
The difference in the holding voltage level at which resonant and non-resonant cells start firing (in a frequency-selective or unselective way, respectively; see **Figure 2F**) might reflect a different voltage window for interaction between  $I_{NaP}$  and  $I_M$ , with the consequent generation of resonant and non-resonant behaviors. To test this possibility, we investigated the degree of interaction between both currents in the same neuron.

### Measurement of Somatic $I_{NaP}$ and $I_M$

We measured  $I_{NaP}$  under voltage clamp by eliciting whole cell currents with a slow voltage ramp (30 mV/s) (Magistretti and Alonso, 1999) to allow  $I_{NaT}$  inactivation, both in control condition and after the application of  $1 \mu\text{M}$  TTX (**Figure 4A**). Then,  $I_{NaP}$  was obtained by digitally subtracting the recording in TTX from the control condition (**Figure 4B**). By this procedure, we obtained a persistent TTX-sensitive current that displayed

non-linear voltage dependence, activated at command potentials above  $-70$  mV and reached peak amplitude near  $-40$  mV (**Figure 4B**). To achieve a better voltage clamp in the presence of  $\text{Na}^+$  currents, in these experiments we decreased the driving force by reducing extracellular  $\text{Na}^+$  concentration (see Section Methods). Therefore, to compare voltage-clamp results with the observations made in current clamp conditions we calculated the persistent  $\text{Na}^+$  conductance ( $G_{NaP}$ ) by dividing the measured current by its driving force ( $V_m - E_{\text{Na}}$ ). The voltage-dependent activation of  $G_{NaP}$  was characterized by fitting a sigmoidal curve to each trace (see Section Methods), obtaining a voltage for half activation ( $V_{0.5}$ ) of  $-52.2 \pm 1.0$  mV, a slope constant of  $4.9 \pm 0.4$  mV and a maximal conductance plateau of  $5.3 \pm 0.5$  nS reached at voltages above  $-40$  mV ( $n = 13$ ; **Figure 4C**). These values are in agreement with previous investigations performed in dissociated CA1 neurons (French et al., 1990) and acute slices (Vervaeke et al., 2006), thus supporting the quality of our measurements. These results show that at perithreshold potential (near  $-58$  mV) a substantial amount of  $G_{NaP}$  is active, thus strongly driving cells toward spike threshold.

Since  $I_M$  is absent at hyperpolarized potentials and activates with depolarization (Halliwell and Adams, 1982), we evoked whole-cell currents by 2 s depolarizing steps from a holding potential of  $-87.5$  mV to voltages between  $-77.5$  and  $-32.5$  mV, with increments of 5 mV. To measure  $I_M$  in the same cells in which we previously measured  $I_{NaP}$ , we applied this



voltage protocol in the presence of TTX as the control condition. The described voltage protocol elicited a sustained whole-cell outward current that contained a combination of several ionic currents (Figure 4D). To isolate  $I_M$  we bath-applied  $10\mu\text{M}$  of the selective blocker XE991 and repeated the protocol after 5–8 mins (Figure 4E), obtaining the XE991-sensitive current by digital subtraction (Figure 4F).

The isolated current showed a slow activation constant (60–200 ms) with no inactivation (Figure 4F), in agreement with the described  $I_M$  kinetics (Shah et al., 2002). The I-V curve shows that the isolated current is inactive at resting potential and begins

to activate above  $-55$  mV, increasing monotonically with voltage and reaching  $\sim 400$  pA at  $-32.5$  mV, the maximal voltage tested (Figure 4G). We computed the  $G$ - $V$  curve dividing the I-V trace by the driving force for  $\text{K}^+$ , obtaining a  $G_M$  curve that appears above  $-60$  mV and reaches  $\sim 6$  nS at  $-32.5$  mV (Figure 4H).

### Comparing Perithreshold Behavior of $I_{\text{NaP}}$ and $I_M$

Once we measured the voltage dependence of  $I_{\text{NaP}}$  and  $I_M$  under the same conditions and in the same cells, we were able to estimate their relative activation levels near perithreshold



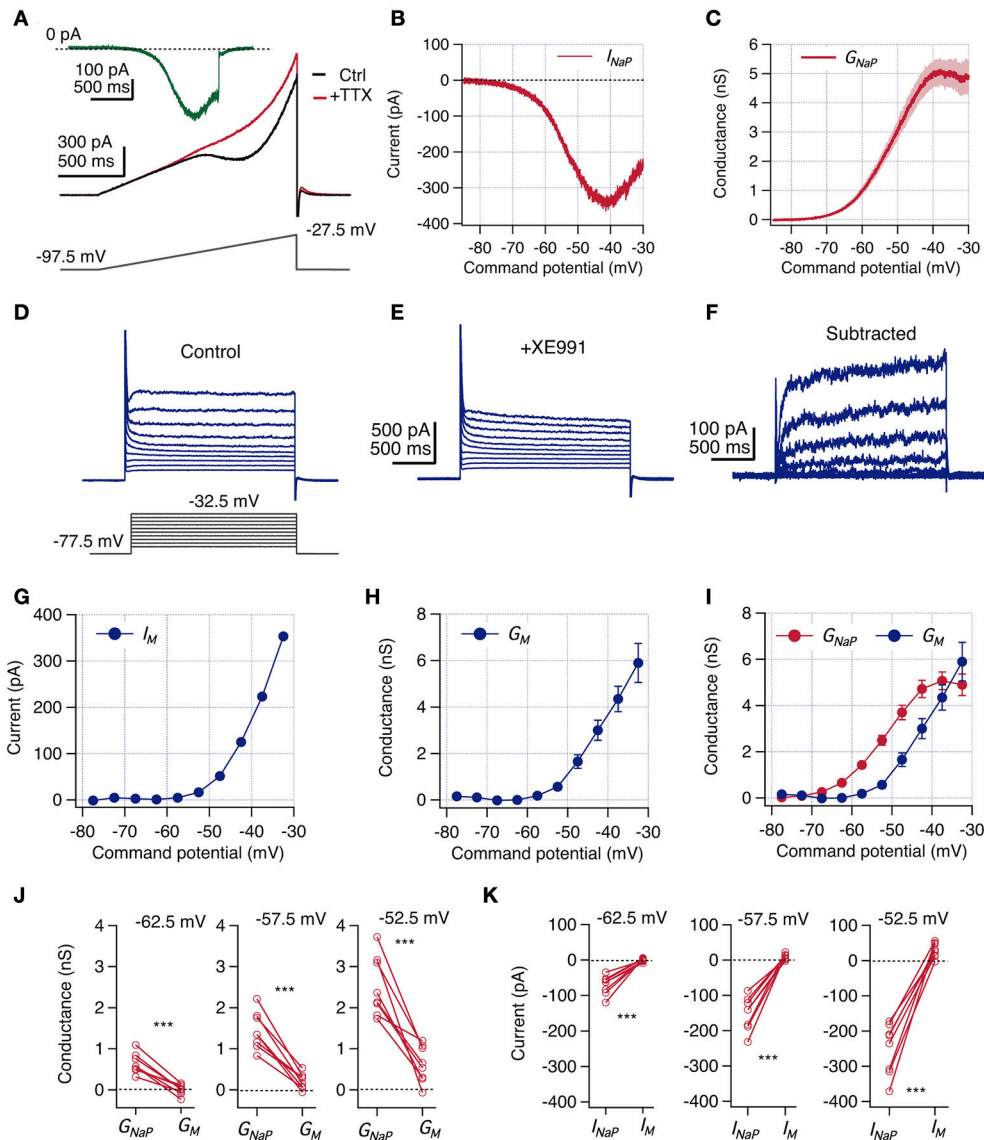
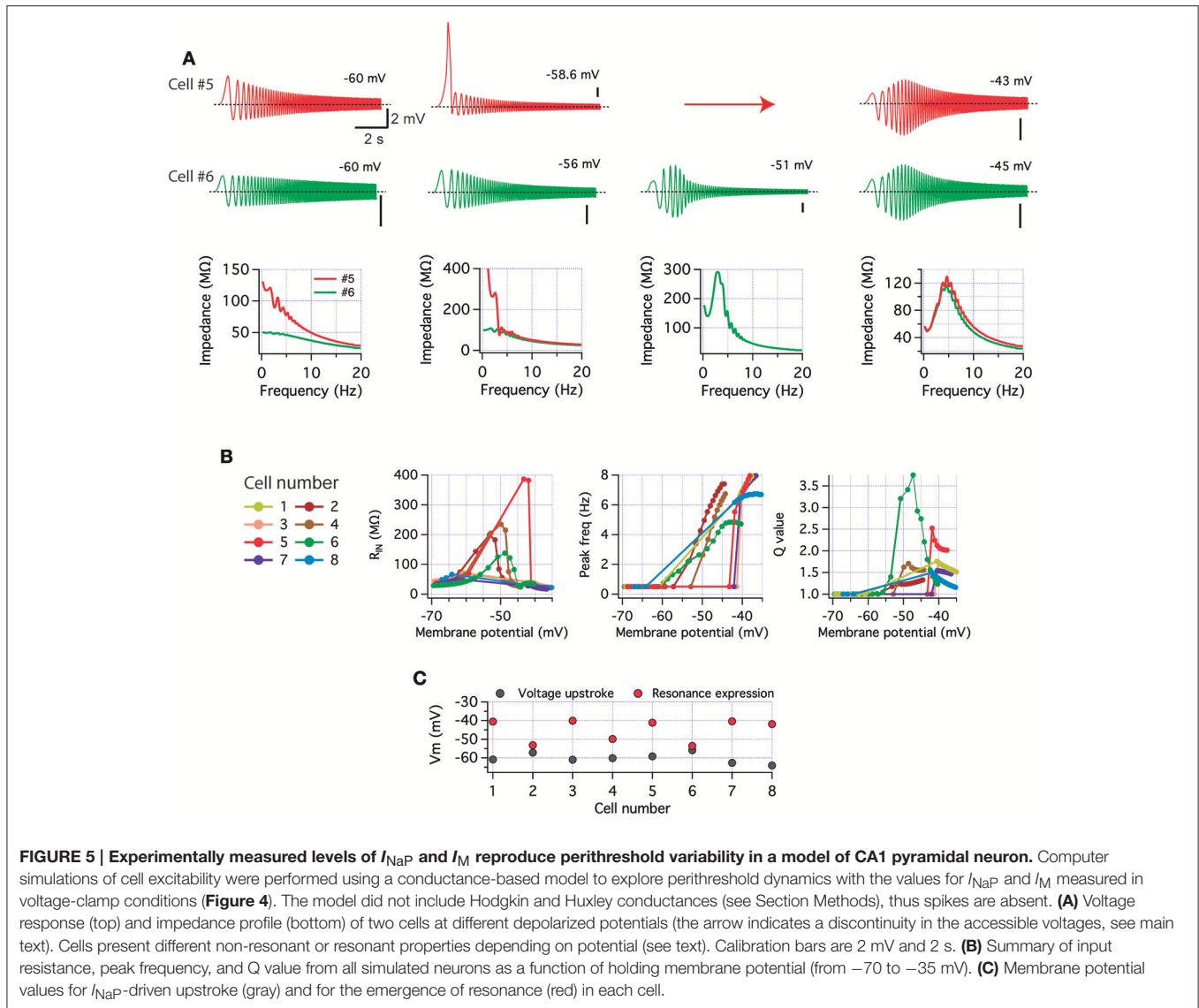


**FIGURE 4 |  $I_{NaP}$  magnitude is larger than  $I_M$  at perithreshold potentials.** Voltage clamp experiments were designed to measure  $I_{NaP}$  and  $I_M$  consecutively in the same CA1 neurons. **(A)** A voltage ramp protocol was used to isolate  $I_{NaP}$  by a subtraction method. The slow depolarizing ramp (46.6 mV/s) inactivates transient  $Na^+$  current in control condition (black) but allows the induction of the persistent current. After addition of 1  $\mu$ M TTX  $I_{NaP}$  is blocked (red). Isolated  $I_{NaP}$  trace is obtained by subtraction of these two recordings (green trace). **(B)** Representative whole-cell  $I_{NaP}$  vs. command potential curve. **(C)** Average  $G_{NaP}$  vs. command potential curve calculated from whole-cell currents curves divided by the driving force ( $V_m - E_{Na}$ ,  $n = 13$ ). **(D,E)** Protocol used to measure  $I_M$ . Neurons were held at  $-87.5$  mV and a family of 2 s depolarizing squared voltage pulses were used to explore potentials between  $-77.5$  and  $-32.5$  with 5 mV steps, at control conditions **(D)** and after bath addition of 10  $\mu$ M of XE991 **(E)**. **(F)**  $I_M$  traces are isolated by subtracting recordings in XE991 from those in control condition. **(G)** Representative whole-cell  $I_M$  vs. command potential obtained from **(F)** (current was measured as the average of the last 50 ms of the pulse response). **(H)** Average  $G_M$  vs. command potential curve ( $n = 13$ ). Individual conductance curves were obtained dividing  $I_M$  by  $V_m - E_K$ . **(I)** Overlap of  $G_{NaP}$  and  $G_M$  curves shown in C and H, respectively. Continue  $G_{NaP}$  curve was quantized extracting values at same potentials explored for  $G_M$ . **(J)** Paired comparison of  $G_{NaP}$  and  $G_M$  obtained at three near threshold potentials ( $n = 8$ ). **(K)** Paired comparison of  $I_{NaP}$  and  $I_M$  calculated using reversal potentials from current clamp condition ( $n = 8$ ). Two-way repeated measures ANOVA, \*\*\* $P < 0.001$ .

potential. Interestingly, the comparison of both curves shows that at all voltages between  $-62.5$  and  $-42.5$  mV,  $G_{NaP}$  is larger than  $G_M$  (Figure 4I). A closer inspection to activated conductances at perithreshold potentials ( $-62.5$ ,  $-57.5$ , and  $-52.5$  mV) shows that in all paired recordings the amount of  $G_{NaP}$  always exceeds  $G_M$ ; with  $G_{NaP}$  ranging from 0.6 to 2.5 nS, whereas  $G_M$  only

reaches a modest average activation of 0.6 nS (See paired values in Figure 4J).

Since at perithreshold potentials the driving force for  $Na^+$  is higher than for  $K^+$ , is expected that the magnitude of the difference between  $I_{NaP}$  and  $I_M$  will be even higher than the difference of their respective conductances. With the driving



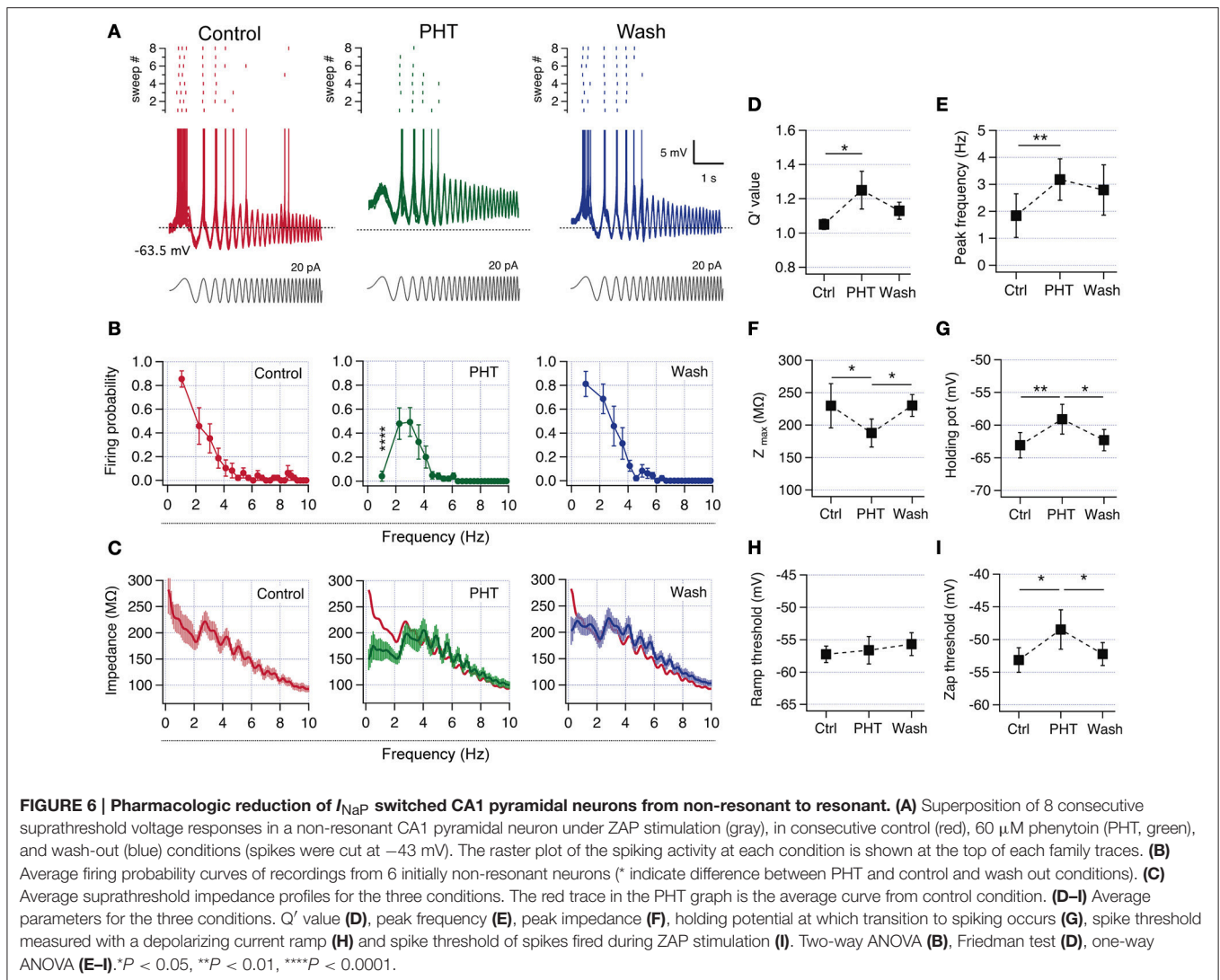
force calculated from the ionic concentrations in our current clamp experiments (see Section Methods) we obtained that  $I_{NaP}$  is around -150 pA at spike threshold levels, while  $I_M$  is only 9 pA, maintaining this paired relative difference for each recorded neuron (See paired values in Figure 4K). These quantifications confirm the reduced contribution of  $I_M$  in the perithreshold region of non-resonant neurons.

### Exploring Perithreshold Behavior with Computer Simulations

To evaluate the expected perithreshold behavior of neurons recorded under voltage clamp we constructed a conductance-based computational model to be applied to each neuron according to their own measured  $I_{NaP}$ ,  $I_M$ , and capacitance (see Section Methods). To gain detail and precision in the computer simulations we fed the model with the specific intrinsic parameters of each cell, instead of using the average

values from a diverse population. As we were interested in evaluating perithreshold frequency preference we did not include in the model the conductances related to action potential generation.

We explored the voltage response to ZAP stimuli for membrane potentials maintained between -70 and -35 mV through injection of a holding current, thus simulating typical current-clamp experiments. Recreated neurons reproduced the variable behavior observed in current clamp experiments, as represented by cells #5 and #6 in Figure 5. Cell #5 displays non-resonant behavior between -70 and -60 mV. However, around the presumed perithreshold potential (near -58 mV), a voltage upstroke of about 10 mV is observed at the first and slowest oscillation of the ZAP, indicating a significant activation of  $I_{NaP}$  (note that a real spike is not seen because Hodgkin & Huxley conductances were omitted in the model; Figure 5A, red). Interestingly, at this point cell #5 holding potential became



unstable, i.e., small increments in holding current generated a step-like transition from  $-58.6$  to  $-43$  mV, a potential at which the neuron stabilizes due to the compensatory effect of  $I_M$  activation, which also generates a strong resonant behavior.

In contrast, cell #6 displays a slight resonant behavior even at presumed perithreshold potentials. Further, current injection produces a gradual depolarization of holding potential accompanied by an increase in resonant behavior, instead of the discontinuous change observed in cell #5 (Figure 5A green). In this second example, the small amount of  $I_M$  activated at perithreshold potential allows the expression of resonance by decreasing voltage oscillations at lower frequencies and preventing the strong depolarization driven by  $I_{NaP}$  in the previous case. Further, co-activation of  $I_{NaP}$  and  $I_M$  by depolarization allows a balanced interplay between both currents that prevents voltage instabilities as in cell #5, producing a strong resonance with depolarization. The impedance profiles for both neurons also show the different behavior at each holding potential (Figure 5A bottom). Note that while responses are

different at perithreshold potential, after depolarization to near  $-40$  mV their impedance profiles are similar. Figure 5B shows the input resistance, peak frequency and resonance strength values against membrane potential for all recreated neurons. An important quality control of the simulations is the reproduction of the increase in input resistance caused by the amplifying effect of  $I_{NaP}$ , and the rise of  $Q$  value attained by  $I_M$  activation. While the general trend was to switch from non-resonant to resonant behavior upon increasing depolarization, resonance appears at different membrane potentials and in most cases following a membrane potential discontinuity as described above (note that this behavior is observed even when holding current increments are as small as 5 pA). As indicated by peak frequency and  $Q$  plots in Figure 5B, transition from non-resonant to resonant behavior is a heterogeneous process with a different voltage point for each neuron. Some neurons transit to depolarized potentials from values as hyperpolarized as  $-60$  mV (cells #1, 3, 7, and 8, Figure 5B). Certainly, this transition is visible in our model due to the absence of spiking activity. In physiological conditions

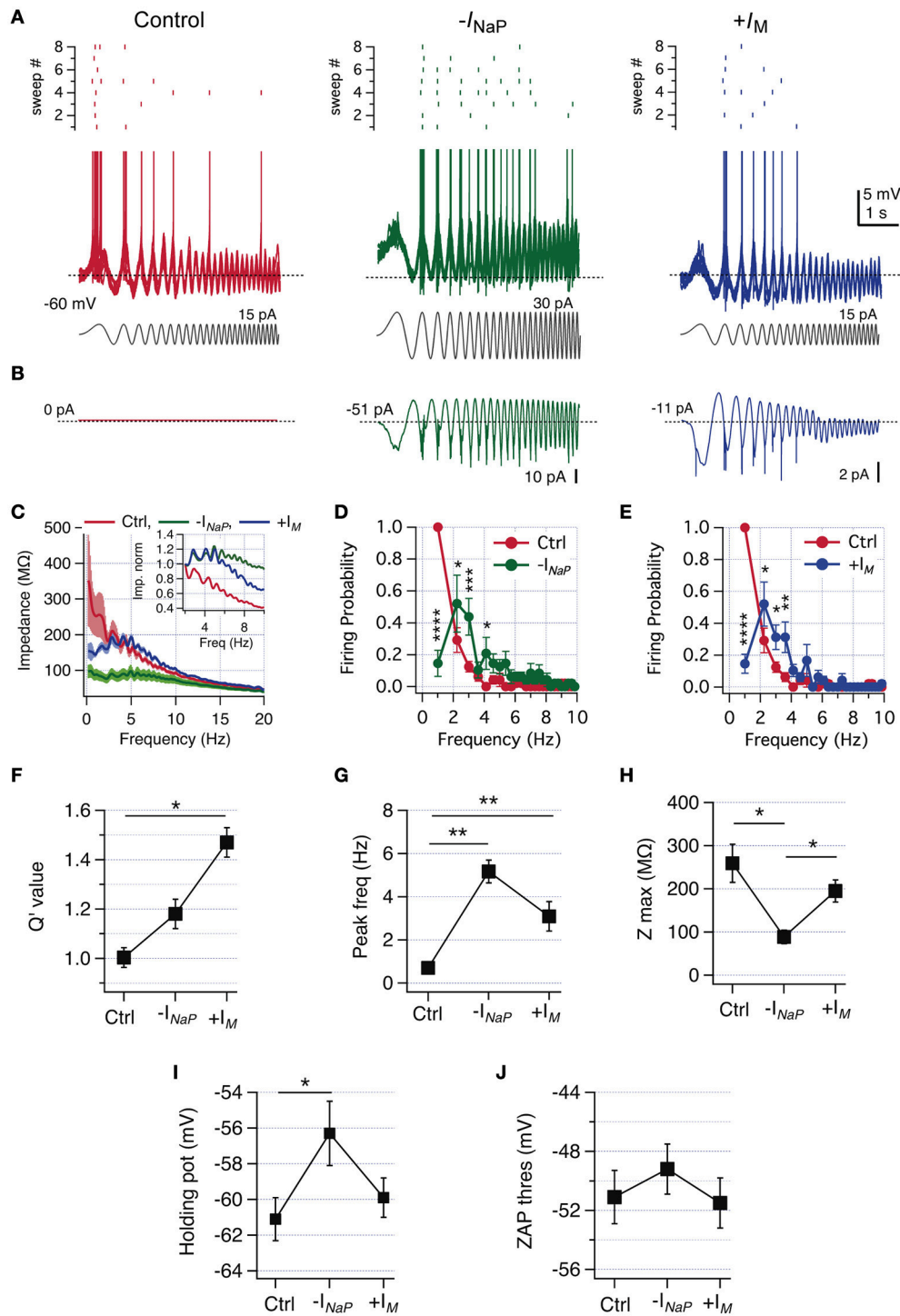


**FIGURE 7 | Reduction of  $I_{NaP}$  or increase of  $I_M$  by dynamic-clamp produces a switch from non-resonant to resonant behavior in CA1 pyramidal neurons.** (A) Superposition of 8 consecutive suprathreshold voltage responses of a non-resonant CA1 pyramidal neuron under ZAP stimulation (gray), in control condition (red) and after virtual canceling of  $I_{NaP}$  ( $-I_{NaP}$ , green) or  $I_M$  increase ( $+I_M$ , blue), by means of dynamic clamping (spikes were cut at  $-43$  mV). The raster plot of the spiking activity at each condition is shown at the top of voltage traces. (B) Average dynamic current injected at each condition, dotted line indicate steady current level. (C) Average impedance profile in control (red),  $-I_{NaP}$  (green) and  $+I_M$  (blue) conditions. Inset, zoom of average curves normalized to the impedance value at 2 Hz (see Section Methods). (D) Average firing probability curves for control (red) and  $-I_{NaP}$  (green) conditions. (E) Average firing probability curves for control (red) and  $+I_M$  (blue) conditions ( $n = 6$ ). (F–J)  $Q'$  value (F), peak frequency (G), peak impedance (H), holding potential for transition to spikes (I) and the spike threshold of the spike fired under ZAP stimulation (J). Two-way repeated measures ANOVA (D,E), Friedman test with Dunn's multiple comparison (G), one-way ANOVA (H–J). \* $P < 0.05$ , \*\* $P < 0.01$ , \*\*\* $P < 0.001$ , \*\*\*\* $P < 0.0001$ .



the transition to resonant behavior in most cases is occluded by the activation of the spiking machinery (as seen in **Figures 1, 2**). It should be noted that the experiments with TTX as those in **Figure 3** are also not comparable with these simulations as this drug not only abolishes action potentials but also block  $I_{\text{NaP}}$ .

To predict the perithreshold behavior of recreated cells, we compared the membrane potential at which  $I_{\text{NaP}}$  activation drives the depolarizing voltage discontinuity (when present) with the membrane potential where resonance is expressed ( $Q > 1$ ). If these two values are close to each other and more hyperpolarized than our measured spike threshold (near  $-52$  mV, **Figure 2**) we considered that neuron as putative resonant (**Figure 5C**). According to this criterion, cells #2 and #6 are putative resonant neurons, while the other 6 neurons are presumed to be non-resonant, in agreement with the abundance of both perithreshold behaviors previously presented (**Figure 1**).

The computational exploration of voltage responses using experimentally measured combinations of  $I_{\text{NaP}}$  and  $I_{\text{M}}$  that constitutes a sample group in the physiological variability of these conductances, supports the idea that the expression of perithreshold resonance depends on their relative magnitudes.

## Inducing Resonant Behavior by Blockade of $I_{\text{NaP}}$

Since we confirmed that all recorded pyramidal neurons have the intrinsic mechanism to display resonant behavior, we now explored if a partial block of  $I_{\text{NaP}}$  can produce resonance in non-resonant neurons. Therefore, we characterized perithreshold behavior and firing preference in control condition, after the addition of  $60 \mu\text{M}$  of the  $I_{\text{NaP}}$  blocker and antiepileptic drug phenytoin (PHT; Chao and Alzheimer, 1995), and after washing out the drug. In control conditions neurons were non-resonant, with a high voltage response and firing probability at the slowest oscillations (**Figure 6A**). When the  $I_{\text{NaP}}$  blocker was added, was necessary to inject more DC current in order to depolarize neurons up to perithreshold potential, compensating the blocking of a depolarizing current (not shown). Moreover, the reduction of  $I_{\text{NaP}}$  also shifts to depolarized values the holding potential necessary to trigger spikes, consistent with a reduction in the intrinsic depolarizing force (note the more depolarized holding potential in **Figures 6A,G**). These changes are accompanied by modifications in the spiking behavior, displaying an attenuated response at low frequencies and a maximal firing probability in the theta range, thus becoming a resonant neuron (**Figure 6A** middle/green). When the drug was washed out the neuron recovered its original non-resonant dynamics (**Figure 6A**,  $n = 6$ ). **Figure 6B** shows the average firing probability curves, indicating that cells moved from a robust low-pass filter behavior at control condition to a band-pass filter pattern when a fraction of  $I_{\text{NaP}}$  is blocked. The effect is almost completely reversed upon blocker removal. The suprathreshold impedance profile in control condition has a low-pass filter shape with a peak impedance of  $233.5 \pm 31 \text{ M}\Omega$  at 1 Hz. Note however that the curve displays a hump near 4 Hz that breaks the monotonic drop of impedance as frequency increases (**Figure 6C**, left). In presence of phenytoin the impedance at 1 Hz falls

below  $200 \text{ M}\Omega$  evidencing the band-pass filter pattern, with the impedance peak at the same frequency of the hump observed in control conditions (see overlapped curves in **Figure 6C**, middle). This change is partially reversed after washing out the drug, and the impedance at 1 Hz grew above  $200 \text{ M}\Omega$ . Regarding resonant parameters, after partial block of  $I_{\text{NaP}}$   $Q'$  rises from  $1.05 \pm 0.03$  to  $1.7 \pm 0.7$ , while  $f_R$  increases from  $1.27 \pm 0.10 \text{ Hz}$  to  $3.6 \pm 0.5 \text{ Hz}$ , consistent with a resonant behavior generated by  $I_{\text{M}}$  (**Figures 6D,E**). In agreement with the amplifying effect of  $I_{\text{NaP}}$ , phenytoin addition produced a 20% drop of peak impedance (**Figure 6F**).

The partial block of  $I_{\text{NaP}}$  produced a raise in the potential at which transition to spiking occurs from  $-63.1 \pm 1.5$  to  $-59 \pm 1.8 \text{ mV}$  (**Figure 6G**), while the spike threshold measured with a voltage ramp was not modified. However, the spike threshold measured when spikes were fired during suprathreshold oscillations suffered a depolarizing shift from  $-54.1 \pm 1.4$  to  $-49.5 \pm 2.3 \text{ mV}$  (**Figures 6H,I**). The transformation of perithreshold behavior induced by phenytoin was partially reverted after drug washout.

These results confirm that non-resonant hippocampal neurons are able to change their firing frequency preference to a resonant behavior by a moderate reduction in  $I_{\text{NaP}}$ .

## Setting Frequency Selectivity through a Sliding Balance between $I_{\text{NaP}}$ and $I_{\text{M}}$

Our following goal was to evaluate the effect of changing the perithreshold balance of  $I_{\text{NaP}}$  and  $I_{\text{M}}$  in non-resonant neurons using dynamic clamp (Dorval et al., 2001). We produced a virtual knock-down of  $I_{\text{NaP}}$  by injecting a negative  $I_{\text{NaP}}$  ( $-I_{\text{NaP}}$ ) to neutralize a fraction of total endogenous  $I_{\text{NaP}}$  (see Section Methods). This strategy is comparable to the previous pharmacological blockade of  $I_{\text{NaP}}$  but now with the possibility to determine the conductance change necessary to produce the switch in perithreshold behavior.

To investigate whether non-resonant neurons are able to resonate with their natural intrinsic levels of  $I_{\text{NaP}}$  in specific conditions, we used dynamic clamp to incorporate a virtual  $I_{\text{M}}$  ( $+I_{\text{M}}$ ) based on the activation curve previously obtained by voltage-clamp experiments, but shifting the voltage sensitivity toward hyperpolarized potentials to increase the voltage window of interaction with  $I_{\text{NaP}}$  (see Section Methods).

We first characterized the frequency preference of a neuron in control condition, corroborating the lack of frequency preference in voltage response and firing probability (**Figure 7A**, left). Then we injected  $-I_{\text{NaP}}$ , beginning with a maximal conductance ( $G_{\text{NaPMax}}$ ) of 2 nS. This amount was enough to observe resonance in three out of six neurons (**Figures 7A-C**). In the other three neurons, it was needed to increase the amount of  $-I_{\text{NaP}}$  to 4.5 nS in one case and to 9 nS in the other two cells to obtain a similar response. Despite the differences in the amount of injected  $-I_{\text{NaP}}$  (canceling an average of  $-147.6 \pm 61.9 \text{ pA}$  of endogenous  $I_{\text{NaP}}$ , not shown), it was possible to induce an equivalent resonant behavior in all 6 neurons, as expressed in the impedance profile (**Figure 7C**) and in the drop of firing probability at low frequencies (**Figure 7D**). Reduction of  $I_{\text{NaP}}$

modified  $Q'$  from 1.0 to  $1.18 \pm 0.06$ , but without reaching statistical significance ( $P = 0.12$ , **Figure 7F**) and shifted  $f_R$  from 0.7 to 5.2 Hz (**Figure 7G**). In agreement with the amplifier role of  $I_{\text{NaP}}$ , its neutralization reduces peak impedance from  $259 \pm 44.1$  to  $88.8 \pm 15.6 \text{ M}\Omega$  (**Figures 7C,H**).

The injection of  $-I_{\text{NaP}}$  depolarizes the holding potential just below threshold from  $-61.1 \pm 1.2$  to  $-56.3 \pm 1.8 \text{ mV}$  (**Figure 7I**) as in phenytoin experiments. Importantly, the modification of  $I_{\text{NaP}}$  did not alter drastically the action potential threshold measured during oscillatory stimulation (**Figure 7J**).

After evaluating the effect of  $-I_{\text{NaP}}$  injection we explored the consequences of injecting  $+I_M$  in the same cells. It was needed to shift the  $V_{0.5}$  of the activation curve from  $-39$  to  $-49 \text{ mV}$  ( $n = 3$ ),  $-54 \text{ mV}$  ( $n = 1$ ) or  $-59 \text{ mV}$  ( $n = 2$ ), to achieve a critical amount of virtual  $I_M$  allowing to change the perithreshold behavior from non-resonant to resonant (average  $+I_M$  current injected during voltage oscillations was  $-20.1 \pm 7.3 \text{ pA}$ , not shown). As expected, intrinsic  $I_{\text{NaP}}$  interacted with  $+I_M$  to induce a perithreshold resonant behavior able to translate frequency preference to spiking regime, with a reduction in firing probability at 1.2 Hz from 1.0 to  $0.15 \pm 0.07$  (**Figure 7E**).  $+I_M$  injection only reduced impedance at frequencies below 4 Hz (**Figure 7C**) and presented a trend to reduce peak impedance (**Figure 7I**). The combination of endogenous high levels of  $I_{\text{NaP}}$  plus a critical amount of  $+I_M$  produces a strong resonant behavior, rising  $Q'$  and shifting average  $f_R$  from  $0.7 \pm 0.2$  to  $3.1 \pm 0.4 \text{ Hz}$  (**Figures 7E,G**). As expected from the unaltered  $I_{\text{NaP}}$ , in the  $+I_M$  condition resonant behavior develops without altering the perithreshold holding membrane potential, nor the spike threshold (**Figures 7I,J**).

Taken together, these results show that the behavior of CA1 pyramidal neurons can be transformed from non-resonant to resonant by changing the relative contributions of  $I_{\text{NaP}}$  and  $I_M$ .

## DISCUSSION

Here we report that CA1 pyramidal neurons present two different types of behaviors when stimulated with an oscillatory current of variable frequency that spans the theta range (0–20 Hz). A small population (20%) of them express perithreshold resonance and fire selectively at theta frequency (4–6 Hz), while the remaining ones (80%) behave as low-pass integrators, i.e., without theta frequency tuning (**Figure 1**). It is important to note that these two behaviors are expressed independently of the hyperpolarized  $I_h$ -resonance (Hu et al., 2002), which was always present (**Figure 1**). These non-resonant neurons preserve their behavior when depolarized until reaching spike threshold, firing spikes with higher probability at the lowest frequencies of stimulation range (**Figure 2**). However, all of these non-resonant cells can display  $I_M$ -driven resonance when depolarized in presence of the  $\text{Na}^+$  channel blocker tetrodotoxin (TTX), suggesting that in regular conditions spike firing at the lowest frequencies precludes the expression of resonance (**Figure 3**). In fact, paired measurement of  $I_{\text{NaP}}$  and  $I_M$  in the same cells showed that at all subthreshold potentials the activation level of  $I_M$  is very low, while  $I_{\text{NaP}}$  is activated enough to depolarize neurons toward spike threshold (**Figure 4**). Computer simulations using the parameters measured in each specific cell in our voltage

clamp experiments support the idea that CA1 pyramidal neurons display heterogeneous contributions of  $I_{\text{NaP}}$  and  $I_M$  and that the expression of perithreshold resonance depends on the interplay between these two conductances (**Figure 5**). Consistent with this possibility, a partial block of  $I_{\text{NaP}}$  with phenytoin or its reduction by dynamic clamp allowed us to change the behavior of non-resonant neurons to resonant (**Figures 6, 7**), demonstrating that different activation levels of  $I_{\text{NaP}}$  can modulate the perithreshold and spiking behavior of a neuron. On the other hand, displacing the activation range for  $I_M$  toward hyperpolarized potentials using dynamic clamp, also transforms non-resonant neurons into resonant (**Figure 7**).

The contribution to single cell excitability of  $I_{\text{NaP}}$  and  $I_M$  has been extensively described in central neurons, but mostly separately.  $I_{\text{NaP}}$  contributes to repetitive firing and to generate rhythmic subthreshold membrane potential oscillations, and also plays a general role as an amplifier current increasing after potential hyperpolarization, synaptic voltage responses (EPSP and IPSP) and promoting resonance (Schwindt and Crill, 1995; Stuart and Sakmann, 1995; Parri and Crunelli, 1998; Stuart, 1999; D'Angelo et al., 2001; Hu et al., 2002; Sanhueza and Bacigalupo, 2005; Vervaeke et al., 2006; Tazerart et al., 2008; Boehlen et al., 2013; Yamada-Hanff and Bean, 2013; Vera et al., 2014).  $I_M$  is the main current involved in frequency accommodation, control of cell excitability, and it has also been described as a current involved in resonance (Hu et al., 2002, 2007; Peters et al., 2005; Lawrence et al., 2006; Shah et al., 2008; Leão et al., 2009; Höningsperger et al., 2015).

Prescott et al. (2008) showed that CA1 pyramidal neurons behave like integrators under *in vitro* conditions (characterized by low synaptic input) and that under *in vivo*-like conditions (under recreated high synaptic stimulation) they switch to resonant behavior by an extrinsically-driven increase of  $I_M$  activation and a secondary depolarization of spike threshold. This switch is a mixed mechanism including intrinsic and synaptic properties and does not explain our observation of resonant behavior under *in vitro* conditions (Hu et al., 2002). Moreover, a recent investigation reported that under muscarine stimulation reducing  $I_M$  and other cationic conductances,  $I_{\text{NaP}}$  drives rhythmic spontaneous firing in CA1 pyramidal neurons (Yamada-Hanff and Bean, 2013), highlighting the relevance of the interaction between  $I_{\text{NaP}}$  and  $I_M$  in controlling cell activity at perithreshold voltage range.

The perithreshold region is an unstable and highly non-linear zone where these currents have opposed effects on membrane potential, with  $I_{\text{NaP}}$  producing depolarization toward spike threshold and promoting an integrator behavior, and  $I_M$  hyperpolarizing the neuron and driving a resonant behavior. It is therefore expected that the precise perithreshold dynamics of CA1 pyramidal neurons should depend on the balance between these two currents. Here we found that in the same conditions and even in the same slice, CA1 pyramidal neurons can behave as non-resonant or resonant relying only on intrinsic properties. We show that at perithreshold potentials  $I_{\text{NaP}}$  displays some degree of variability in activation among the recorded neurons, whereas  $I_M$  is mostly inactive (**Figures 4I–K**). However, small amounts of activated  $I_M$  will allow resonance expression (**Figures 5, 7**). For this reason, we propose that the

perithreshold behavior of CA1 pyramidal neurons is variable and its specific shape will depend on the relative levels of  $I_{\text{NaP}}$  and  $I_{\text{M}}$  given by their particular values of maximal conductances and voltage sensitivities. Thus, perithreshold behavior of CA1 pyramidal neurons lies on a continuum between two extreme configurations. At one extreme are those neurons in which  $I_{\text{NaP}}$  activation begins at relatively hyperpolarized potentials, setting a steady state perithreshold voltage below activation ranges for  $I_{\text{M}}$  and displaying a strong non-resonant behavior. Whereas in the other extreme are those neurons in which low levels of  $I_{\text{NaP}}$  induce a slow depolarization that inactivates a fraction of  $I_{\text{NaT}}$  and also of  $I_{\text{NaP}}$  (Colombo et al., 2013), reaching a more depolarized steady state potential and concomitant shift of spike threshold to positive values (Fernandez and White, 2010). This depolarized perithreshold potential allows  $I_{\text{M}}$  activation and the expression of resonant behavior. According to this, all CA1 pyramidal neurons have the intrinsic ability to display perithreshold frequency tuning, but the expression of this property would depend on whether the level of  $I_{\text{NaP}}$  allows significant  $I_{\text{M}}$  activation before spiking is triggered. Conversely, those neurons where perithreshold levels of  $I_{\text{M}}$  are high enough to counterbalance  $I_{\text{NaP}}$ -driven depolarization will filter low frequency oscillations and express resonant behavior.

Our experiments with pharmacology and dynamic clamping demonstrate that reducing the amount of  $I_{\text{NaP}}$  or increasing  $I_{\text{M}}$  is enough to change the behavior of one neuron from non-resonant to resonant. Given the subtle change needed to transform the perithreshold behavior, it is plausible that in the intact brain neurons can switch between these behaviors due to the modulation of current amplitude and/or voltage sensitivity by intracellular second messengers or neuromodulators. In fact, both currents are highly regulated, with  $I_{\text{NaP}}$  being modulated in amplitude and/or voltage sensitivity by PKC (Astman et al., 1998), dopamine receptor activation (Gorelova and Yang, 2000), oxidative metabolism (Hammarstrom and Gage, 1998) and G-protein subunits composition (Ma et al., 1997; Mantegazza et al., 2005), and  $I_{\text{M}}$  being suppressed by activation of muscarinic receptors (Delmas and Brown, 2005) and by endocannabinoids (Schweitzer, 2000) or increased by somatostatin (Moore et al., 1988). Moreover, muscarinic receptor activation may directly modulate  $I_{\text{NaP}}$  (Mittmann and Alzheimer, 1998). This degree of modulation may be, at least in part, the reason why some authors have described the behavior of CA1 pyramidal neurons at perithreshold potential as integrators and others as resonators (discussed in Hu et al., 2002). Thus, the observation of distinct excitability profiles within the same cell type is highly expected.

The fact that we found different perithreshold behavior in the same experimental conditions, with the control of intracellular metabolites concentration and the composition of extracellular recording solution, suggests that one possible cause of the differential behavior relies on the specific quantities of  $\text{Na}_V$  and  $\text{KCNQ}$  channels expressed at each neuron. This is in agreement with the current view of cell excitability, in which the level of expression of each conductance varies from cell to cell, producing heterogeneous mixes of membrane conductances that

would shape the specific behavior of a neuron (Destexhe and Marder, 2004; Marder and Goaillard, 2006). Thus, together with the transient modulation of  $I_{\text{NaP}}$  and  $I_{\text{M}}$ , there is a structural variability that sets a specific subthreshold behavior of neurons when observed under controlled conditions.

Finally, we propose that CA1 neurons are endowed with the intrinsic ability to switch between non-resonant and resonant behavior through a sliding balance of  $I_{\text{NaP}}$  and  $I_{\text{M}}$ . Considering that the behavior of the neurons at perithreshold potentials has a tremendous influence in the way neurons translate subthreshold activity to action potentials, this intrinsic switching mechanism might dynamically tune responsiveness of neurons favoring the processing of specific rhythms. The fact that both currents are highly modulated by intracellular signals and neuromodulators (Moore et al., 1988; Ma et al., 1997; Astman et al., 1998; Hammarstrom and Gage, 1998; Gorelova and Yang, 2000; Schweitzer, 2000; Delmas and Brown, 2005; Mantegazza et al., 2005) can introduce a fast mechanism of perithreshold frequency tuning in CA1 hippocampus favoring selective firing at theta rhythm. Furthermore, since  $I_{\text{NaP}}$  (Stafstrom, 2007) and  $I_{\text{M}}$  (Halliwell, 1986) are expressed in most cortical neurons, the mechanism described here is possibly a more general strategy to control selective firing under oscillatory synaptic input.

## AUTHOR CONTRIBUTIONS

JV and MS conceived and designed the experiments, JV performed the experiments and developed the computational model. JV and JA analyzed the data. JA and MS contributed reagents/materials/analysis tools. JV, JA, and MS wrote the paper.

## FUNDING

Fondo Nacional de Desarrollo Científico y Tecnológico (FONDECYT) 1140700 (MS), 3150668 (JV) and 1130177 (JA).

## ACKNOWLEDGMENTS

We thank to Pablo Vergara, Ethan Guthman, Chris Chen and Michael Wallace for critical comments on the manuscript.

## SUPPLEMENTARY MATERIAL

The Supplementary Material for this article can be found online at: <http://journal.frontiersin.org/article/10.3389/fncel.2017.00061/full#supplementary-material>

**Figure S1 | Quantification of Q-value, frequency of preference and peak impedance in CA1 neurons.** Raw data from analysis shown in **Figure 1**. **(A–C)** Average values (filled circles) vs. membrane potential shown in **Figure 1C**, with the addition of the data from single experiments (rectangles). Resonant (Res,  $n = 5$ ) and non-resonant (Non,  $n = 21$ ) neurons are defined according to their Q value at depolarized subthreshold potential (Methods). **(D–F)**. In order to facilitate visual analysis of the raw data, we plotted same data as in **(A–C)** defining three ranges of membrane potential: hyperpolarized (Hyp,  $\sim -85$  mV), near resting (Res,  $\sim -70$  mV), and depolarized (Dep,  $\sim -63$  mV), for resonant (Res,  $n = 5$ ) and non-resonant (Non,  $n = 21$ ) neurons.



## REFERENCES

- Adams, P. R., Brown, D. A., and Constanti, A. (1982). M-currents and other potassium currents in bullfrog sympathetic neurones. *J. Physiol.* 330, 537–572. doi: 10.1113/jphysiol.1982.sp014357
- Astman, N., Gutnick, M. J., and Fleidervish, I. A. (1998). Activation of Protein Kinase C increases neuronal excitability by regulating persistent Na<sup>+</sup> current in mouse neocortical slices. *J. Neurophysiol.* 80, 1547–1551.
- Bettencourt, J. C., Lillis, K. P., Stupin, L. R., and White, J. A. (2008). Effects of imperfect dynamic clamp: computational and experimental results. *J. Neurosci. Methods* 169, 282–289. doi: 10.1016/j.jneumeth.2007.10.009
- Biel, M., Wahl-schott, C., Michalakis, S., and Zong, X. (2009). Hyperpolarization-activated cation channels: from genes to function. *Physiol. Rev.* 89, 847–885. doi: 10.1152/physrev.00029.2008
- Boehlen, A., Henneberger, C., Heinemann, U., and Erchova, I. (2013). Contribution of near-threshold currents to intrinsic oscillatory activity in rat medial entorhinal cortex layer II stellate cells. *J. Neurophysiol.* 109, 445–463. doi: 10.1152/jn.00743.2011
- Buzsáki, G. (2002). Theta oscillations in the hippocampus. *Neuron* 33, 325–340. doi: 10.1016/S0896-6273(02)00586-X
- Buzsáki, G. (2005). Theta rhythm of navigation: link between path integration and landmark navigation, episodic and semantic memory. *Hippocampus* 15, 827–840. doi: 10.1002/hipo.20113
- Chao, T., and Alzheimer, C. (1995). Effects of phenytoin on the persistent Na current. *Neuroreport* 6, 1778–1780. doi: 10.1097/00001756-199509000-00017
- Colombo, E., Franceschetti, S., Avanzini, G., and Mantegazza, M. (2013). Phenytoin inhibits the persistent sodium current in neocortical neurons by modifying its inactivation properties. *PLoS ONE* 8:e55329. doi: 10.1371/journal.pone.0055329
- Crill, W. E. (1996). Persistent sodium current in mammalian central neurons. *Annu. Rev. Physiol.* 58, 349–362. doi: 10.1146/annurev.ph.58.030196.002025
- D'Angelo, E., De Filippi, G., Rossi, P., and Taglietti, V. (1998). Ionic mechanism of electroresponsiveness in cerebellar granule cells implicates the action of a persistent sodium current. *J. Neurophysiol.* 80, 493–503.
- D'Angelo, E., Nieus, T., Maffei, A., Armano, S., Rossi, P., Taglietti, V. et al. (2001). Theta-frequency bursting and resonance in cerebellar granule cells: experimental evidence and modeling of a slow k<sup>+</sup>-dependent mechanism. *J. Neurosci.* 21, 759–770.
- Delmas, P., and Brown, D. A. (2005). Pathways modulating neural KCNQ/M (Kv7) potassium channels. *Nat. Rev. Neurosci.* 6, 850–862. doi: 10.1038/nrn1785
- Destexhe, A., and Marder, E. (2004). Plasticity in single neuron and circuit computations. *Nature* 431, 789–795. doi: 10.1038/nature03011
- Dorval, A. D., Christini, D. J., and White, J. A. (2001). Real-time linux dynamic clamp: a fast and flexible way to construct virtual ion channels in living cells. *Ann. Biomed. Eng.* 29, 897–907. doi: 10.1114/1.1408929
- Fernandez, F. R., and White, J. A. (2010). Gain control in CA1 pyramidal cells using changes in somatic conductance. *J. Neurosci.* 30, 230–241. doi: 10.1523/JNEUROSCI.3995-09.2010
- French, C. R., Sah, P., Buckett, K. J., and Gage, P. W. (1990). A voltage-dependent persistent sodium current in mammalian hippocampal neurons. *J. Gen. Physiol.* 95, 1139–1157. doi: 10.1085/jgp.95.6.1139
- Golowasch, J., Thomas, G., Taylor, A. L., Patel, A., Pineda, A., Khalil, C. et al. (2009). Membrane Capacitance measurements revisited: Dependence of capacitance value on measurement method in nonisopotential neurons. *J. Neurophysiol.* 102, 2161–2175. doi: 10.1152/jn.00160.2009
- Gorelova, N. A., and Yang, C. R. (2000). Dopamine D1 / D5 receptor activation modulates a persistent sodium current in rat prefrontal cortical neurons *in vitro*. *J. Neurophysiol.* 84, 75–87.
- Gutfreund, Y., Yarom, Y., and Segev, I. (1995). Subthreshold oscillations and resonant frequency in guinea-pig cortical neurons: physiology and modelling. *J. Physiol.* 483(pt 3), 621–640. doi: 10.1113/jphysiol.1995.sp020611
- Halliwel, J. (1986). M-Current in human neocortical neurones. *Neurosci. Lett.* 67, 1–6. doi: 10.1016/0304-3940(86)90198-9
- Halliwel, J., and Adams, P. (1982). Voltage-clamp analysis of muscarinic excitation in hippocampal neurons. *Brain Res.* 250, 71–92. doi: 10.1016/0006-8993(82)90954-4
- Hammarstrom, A. K. M., and Gage, P. W. (1998). Inhibition of oxidative metabolism increases persistent sodium current in rat CA1 hippocampal neurons. *J. Physiol.* 510, 735–741. doi: 10.1111/j.1469-7793.1998.735bj.x
- Hodgkin, A. L., and Huxley, A. F. (1952). A quantitative description of membrane current and its application to conduction and excitation in nerve. *J. Physiol.* 117, 500–544. doi: 10.1113/jphysiol.1952.sp004764
- Hönigsperger, C., Marosi, M., Murphy, R., and Storm, J. F. (2015). Dorsoventral differences in Kv7/M-current and its impact on resonance, temporal summation and excitability in rat hippocampal pyramidal cells. *J. Physiol.* 593, 1551–1580. doi: 10.1113/jphysiol.2014.280826
- Hu, H., Vervaeke, K., Graham, L. J., and Storm, J. F. (2009). Complementary theta resonance filtering by two spatially segregated mechanisms in CA1 hippocampal pyramidal neurons. *J. Neurosci.* 29, 14472–14483. doi: 10.1523/JNEUROSCI.0187-09.2009
- Hu, H., Vervaeke, K., and Storm, J. F. (2002). Two forms of electrical resonance at theta frequencies, generated by M-current, h-current and persistent Na<sup>+</sup> current in rat hippocampal pyramidal cells. *J. Physiol.* 545, 783–805. doi: 10.1113/jphysiol.2002.029249
- Hu, H., Vervaeke, K., and Storm, J. F. (2007). M-channels (Kv7/KCNQ channels) that regulate synaptic integration, excitability, and spike pattern of CA1 pyramidal cells are located in the perisomatic region. *J. Neurosci.* 27, 1853–1867. doi: 10.1523/JNEUROSCI.4463-06.2007
- Hutcheon, B., Miura, R. M., and Pail, E. (1996). Subthreshold membrane resonance in neocortical neurons. *J. Neurophysiol.* 76, 698–714.
- Hutcheon, B., and Yarom, Y. (2000). Resonance, oscillation and the intrinsic frequency preferences of neurons. *Trends Neurosci.* 23, 216–222. doi: 10.1016/S0166-2236(00)01547-2
- Izhikevich, E. M. (2002). Resonance and selective communication via bursts in neurons having subthreshold oscillations. *BioSystems* 67, 95–102. doi: 10.1016/S0303-2647(02)00067-9
- Kaczorowski, C. C., Disterhoft, J., and Spruston, N. (2011). Stability and plasticity of intrinsic membrane properties in hippocampal CA1 pyramidal neurons: effects of internal anions. *J. Physiol.* 3, 799–818. doi: 10.1113/jphysiol.2006.124586
- Kearney, J. A., Plummer, N. W., Smith, M. R., Kapur, J., Cummins, T. R., Waxman, S. G. et al. (2001). A gain-of-function mutation in the sodium channel gene *Scn2a* results in seizures and behavioral abnormalities. *Neuroscience* 102, 307–317. doi: 10.1016/S0306-4522(00)00479-6
- Koch, C. (1984). Cable theory in neurons with active, linearized membranes. *Biol. Cybern.* 50, 15–33. doi: 10.1007/BF00317936
- Lawrence, J. J., Saraga, F., Churchill, J. F., Statland, J. M., Travis, K. E., Skinner, F. K. et al. (2006). Somatodendritic Kv7/KCNQ/M channels control interspike interval in hippocampal interneurons. *J. Neurosci.* 26, 12325–12338. doi: 10.1523/JNEUROSCI.3521-06.2006
- Leão, R. N., Tan, H. M., and Fisahn, A. (2009). Kv7/KCNQ channels control action potential phasing of pyramidal neurons during hippocampal gamma oscillations *in vitro*. *J. Neurosci.* 29, 13353–13364. doi: 10.1523/JNEUROSCI.1463-09.2009
- Lisman, J. (2005). The theta/gamma discrete phase code occurring during the hippocampal phase precession may be a more general brain coding scheme. *Hippocampus* 15, 913–922. doi: 10.1002/hipo.20121
- Ma, J. Y., Catterall, W. A., and Scheuer, T. (1997). Persistent sodium currents through brain sodium channels induced by G protein  $\beta\gamma$  subunits. *Neuron* 19, 443–452. doi: 10.1016/S0896-6273(00)80952-6
- Magee, J. C. (1998). Dendritic hyperpolarization-activated currents modify the integrative properties of hippocampal CA1 pyramidal neurons. *J. Neurosci.* 18, 7613–7624.
- Magistretti, J., and Alonso, A. (1999). Biophysical properties and slow voltage-dependent inactivation of a sustained sodium current in entorhinal cortex layer-II principal neurons: a whole-cell and single-channel study. *J. Gen. Physiol.* 114, 491–509. doi: 10.1085/jgp.114.4.491
- Mantegazza, M., Yu, F. H., Powell, A. J., Clare, J. J., Catterall, W. A., and Scheuer, T. (2005). Molecular determinants for modulation of persistent sodium current by G-protein betagamma subunits. *J. Neurosci.* 25, 3341–3349. doi: 10.1523/JNEUROSCI.0104-05.2005
- Marder, E., and Goaillard, J.-M. (2006). Variability, compensation and homeostasis in neuron and network function. *Nat. Rev. Neurosci.* 7, 563–574. doi: 10.1038/nrn1949



- Marrion, N. V. (1997). Control of M-Current. *Annu. Rev. Physiol.* 59, 483–504. doi: 10.1146/annurev.physiol.59.1.483
- Mittmann, T., and Alzheimer, C. (1998). Muscarinic inhibition of persistent Na<sup>+</sup> current in rat neocortical pyramidal neurons. *J. Neurophysiol.* 79, 1579–1582.
- Moore, S. D., Madamba, S. G., Joels, M., and Siggins, G. R. (1988). Somatostatin augments the M-Current in Hippocampal Neurons. *Science* 239, 278–280. doi: 10.1126/science.2892268
- Neher, E. (1992). Correction for liquid junction potentials in patch clamp experiments. *Meth. Enzymol.* 207, 123–131. doi: 10.1016/0076-6879(92)07008-C
- O'Keefe, J., and Recce, M. (1993). Phase relationship between hippocampal place units and the hippocampal theta rhythm. *Hippocampus* 3, 317–330.
- Parri, H. R., and Crunelli, V. (1998). Sodium current in rat and cat thalamocortical neurons: role of a non-inactivating component in tonic and burst firing. *J. Neurosci.* 18, 854–867.
- Peters, H. C., Hu, H., Pongs, O., Storm, J. F., and Isbrandt, D. (2005). Conditional transgenic suppression of M channels in mouse brain reveals functions in neuronal excitability, resonance and behavior. *Nat. Neurosci.* 8, 51–60. doi: 10.1038/nn1375
- Prescott, S. A., Ratté, S., De Koninck, Y., and Sejnowski, T. J. (2008). Pyramidal neurons switch from integrators *in vitro* to resonators under *in vivo* conditions. *J. Neurophysiol.* 100, 3030–3042. doi: 10.1152/jn.90634.2008
- Sanhueza, M., and Bacigalupo, J. (2005). Intrinsic subthreshold oscillations of the membrane potential in pyramidal neurons of the olfactory amygdala. *Eur. J. Neurosci.* 22, 1618–1626. doi: 10.1111/j.1460-9568.2005.04341.x
- Schweitzer, P. (2000). Cannabinoids Decrease the K<sup>+</sup> M-Current in Hippocampal CA1 Neurons. *J. Neurosci.* 20, 51–58.
- Schwindt, P. C., and Crill, W. E. (1995). Amplification of synaptic current by persistent sodium conductance in apical dendrite of neocortical neurons. *J. Neurophysiol.* 74, 2220–2224.
- Shah, M. M., Migliore, M., Valencia, I., Cooper, E. C., and Brown, D. A. (2008). Functional significance of axonal Kv7 channels in hippocampal pyramidal neurons. *Proc. Natl. Acad. Sci. U.S.A.* 105, 7869–7874. doi: 10.1073/pnas.0802805105
- Shah, M. M., Mistry, M., Marsh, S. J., Brown, D. A and Delmas, P. (2002). Molecular correlates of the M-current in cultured rat hippocampal neurons. *J. Physiol.* 544, 29–37. doi: 10.1113/jphysiol.2002.028571
- Stafstrom, C. E. (2007). Persistent sodium current and its role in epilepsy. *Epilepsy Curr.* 7, 15–22. doi: 10.1111/j.1535-7511.2007.00156.x
- Stuart, G. (1999). Voltage-activated sodium channels amplify inhibition in neocortical pyramidal neurons. *Nature* 2, 144–150.
- Stuart, G., and Sakmann, B. (1995). Amplification of EPSPs by axosomatic sodium channels in neocortical pyramidal neurons. *Neuron* 15, 1065–1076. doi: 10.1016/0896-6273(95)90095-0
- Tazerart, S., Vinay, L., and Brocard, F. (2008). The persistent sodium current generates pacemaker activities in the central pattern generator for locomotion and regulates the locomotor rhythm. *J. Neurosci.* 28, 8577–8589. doi: 10.1523/JNEUROSCI.1437-08.2008
- Vera, J., Pezzoli, M., Pereira, U., Bacigalupo, J., and Sanhueza, M. (2014). Electrical resonance in the  $\theta$  frequency range in olfactory amygdala neurons. *PLoS ONE* 9:e85826. doi: 10.1371/journal.pone.0085826
- Vervaeke, K., Hu, H., Graham, L. J., and Storm, J. F. (2006). Contrasting effects of the persistent Na<sup>+</sup> current on neuronal excitability and spike timing. *Neuron* 49, 257–270. doi: 10.1016/j.neuron.2005.12.022
- Wang, H. S., Pan, Z., Shi, W., Brown, B. S., Wymore, R. S., Cohen, I. S. et al. (1998). KCNQ2 and KCNQ3 potassium channel subunits: molecular correlates of the M-channel. *Science* 282, 1890–1893. doi: 10.1126/science.282.5395.1890
- Xu, J., Kang, N., Jiang, L., Nedergaard, M., and Kang, J. (2005). Activity-dependent long-term potentiation of intrinsic excitability in hippocampal CA1 pyramidal neurons. *J. Neurosci.* 25, 1750–1760. doi: 10.1523/JNEUROSCI.4217-04.2005
- Yamada-Hanff, J., and Bean, B. P. (2013). Persistent sodium current drives conditional pacemaking in CA1 pyramidal neurons under muscarinic stimulation. *J. Neurosci.* 33, 15011–15021. doi: 10.1523/JNEUROSCI.0577-13.2013

**Conflict of Interest Statement:** The authors declare that the research was conducted in the absence of any commercial or financial relationships that could be construed as a potential conflict of interest.

Copyright © 2017 Vera, Alcayaga and Sanhueza. This is an open-access article distributed under the terms of the Creative Commons Attribution License (CC BY). The use, distribution or reproduction in other forums is permitted, provided the original author(s) or licensor are credited and that the original publication in this journal is cited, in accordance with accepted academic practice. No use, distribution or reproduction is permitted which does not comply with these terms.